Symmetry analysis of light-induced magnetic interactions via Floquet engineering

Ryota Yambe [1,*] and Satoru Hayami [2,†]

[1]*Department of Applied Physics, The University of Tokyo, Tokyo 113-8656, Japan*
[2]*Graduate School of Science, Hokkaido University, Sapporo 060-0810, Japan*

Anisotropic magnetic interactions become the origins of intriguing magnetic structures, such as helical and skyrmion structures by the Dzyaloshinskii-Moriya interaction. In general, possible anisotropic exchange interactions are restricted by crystal symmetry. Meanwhile, by lowering the crystal symmetry with light, additional anisotropic magnetic interactions are expected according to its polarization and frequency. In this study, we clarify a relation between anisotropic magnetic interactions and symmetry lowering in insulating magnets irradiated by light. Based on the Floquet formalism, we find that a variety of anisotropic two-spin and three-spin interactions are induced via spin-dependent electric polarizations activated by light irrespective of the presence/absence of the space inversion symmetry; we systematically classify them in the hexagonal point groups, tetragonal point groups, and their subgroups. Our symmetry analyses show that the light-induced two-spin (three-spin) interactions are due to the reduction of the point group to a chiral point group (black and white magnetic point group). We also demonstrate the effect of the light-induced magnetic interactions on the magnetic structures in a triangular unit. Our results will be a symmetry-based reference for the Floquet engineering of magnetic structures.

I. INTRODUCTION

Floquet engineering of physical properties has attracted much attention in various fields of condensed matter physics, which gives us a framework to understand the time evolution driven by a time-periodic field within a time-independent Hamiltonian [1–3]. In magnetic systems, the effect of such a time-periodic field appears in the modification of magnetic interactions, which results in a variety of phase transitions and associated material design. For example, a periodic electric field to the Mott insulator brings about the change of the sign and amplitude of exchange interactions [4–10] and the induction of multiple-spin interactions [11–14] depending on the intensity, polarization, and frequency of the light. Moreover, combined with the effect of the spin-orbit coupling, the control of anisotropic exchange interactions by light is possible, as demonstrated in the noncentrosymmetric magnet [15] and the Kitaev magnet [16–20].

In general, possible anisotropic exchange interactions are restricted by the crystal symmetry. For example, the Dzyaloshinskii-Moriya (DM) interaction [21,22] appears only when the space inversion symmetry in the lattice structure is absent. Thus, it is difficult to control the type of anisotropic exchange interactions once the crystal symmetry is determined. Meanwhile, by introducing the external field, one can expect various symmetry lowerings depending on the direction and polarization of the light, which gives rise to additional anisotropic exchange interactions that are prohibited in the

underlying lattice structure. This leads to the possibility of engineering any magnetic structures with desired functionalities, which will provide a new guideline for Floquet engineering of the magnetic structures.

This paper gives a symmetry-based understanding of light-induced anisotropic magnetic interactions. Based on the Floquet formalism in previous studies [23,24], we show that a spin-dependent electric polarization activated by light can be the origin of various types of anisotropic magnetic interactions, such as anisotropic two-site two-spin interactions, anisotropic two-site three-spin interactions, and anisotropic three-site three-spin interactions, by performing group-theory and perturbation analyses. We classify the light-induced magnetic interactions for the hexagonal point groups, tetragonal point groups, and their subgroups in a systematic manner. As a result, we show a comprehensive correspondence between the emergent magnetic interactions and symmetry lowering by light. We also demonstrate that the light-induced magnetic interactions favor a noncoplanar spin structure with nonzero spin scalar chirality on a triangular unit even without an external static magnetic field. Our symmetry analysis of the light-induced magnetic interactions will be a reference for controlling magnetic structures by light.

The rest of this paper is organized as follows. We introduce a static model and time-dependent light-driven model in Secs. II A and II B, respectively. We show that the time-dependent model is mapped onto effective time-independent magnetic interactions by using Floquet theory in Sec. II C. We present symmetry-based understanding of the light-induced two-site two-spin interaction, two-site three-spin interaction, and three-site three-spin interaction under crystallographic point groups in Secs. III A–III C. We apply the result to a

system consisting of a triangular unit in Sec. IV. We summa-
rize the paper in Sec. V.

II. MODEL

A. Static Hamiltonian

We consider a spin model with a generalized bilinear ex-
change interaction without time dependence, which is given
by

$$\mathcal{H}_0 = \sum_{i,j} \sum_{\alpha,\beta} J_{ij}^{\alpha\beta} S_i^\alpha S_j^\beta, \tag{1}$$
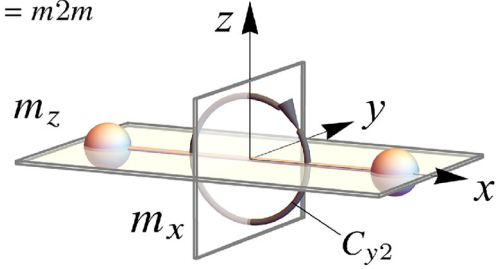
with

$$J_{ij} = \begin{pmatrix} F_{ij}^x & E_{ij}^z + D_{ij}^z & E_{ij}^y - D_{ij}^y \\ E_{ij}^z - D_{ij}^z & F_{ij}^y & E_{ij}^x + D_{ij}^x \\ E_{ij}^y + D_{ij}^y & E_{ij}^x - D_{ij}^x & F_{ij}^z \end{pmatrix}. \tag{2}$$

Here, $\mathbf{S}_i = (S_i^x, S_i^y, S_i^z)$ is the quantum spin operator with ar-
bitrary spin length at site i, the summation is taken over
the bonds in the target lattice structure, and $\alpha, \beta = x, y, z$.
The coupling matrix J_{ij} has nine independent components
in each $\langle i, j \rangle$ bond: three antisymmetric off-diagonal com-
ponents $\mathbf{D}_{ij} = (D_{ij}^x, D_{ij}^y, D_{ij}^z)$, three symmetric off-diagonal
components $\mathbf{E}_{ij} = (E_{ij}^x, E_{ij}^y, E_{ij}^z)$, and three symmetric di-
agonal components $\mathbf{F}_{ij} = (F_{ij}^x, F_{ij}^y, F_{ij}^z)$. The antisymmetric
(symmetric) components are odd (even) with respect to the
interchange of two sites: $\mathbf{D}_{ij} = -\mathbf{D}_{ji}$, $\mathbf{E}_{ij} = \mathbf{E}_{ji}$, and $\mathbf{F}_{ij} =
\mathbf{F}_{ji}$. The exchange interaction with $J_{ij}^{\mathrm{iso}} = (F_{ij}^x + F_{ij}^y + F_{ij}^z)/3$
is isotropic in spin space, while D_{ij}^α, E_{ij}^α, and $F_{ij}^\alpha - J_{ij}^{\mathrm{iso}}$
are anisotropic in spin space. The anisotropic exchange

TABLE I. Symmetry analysis of J_{12}, Y_{12}^x, and Y_{12}^y for the $\langle 1, 2 \rangle$
bond along the x direction on the xy plane under 15 point groups. In
the point group $\mathbf{G}$, the first, second, and third axes are taken along the
$x, y,$ and z directions, respectively. $\parallel \sharp (\perp \sharp)$ for $\sharp = \hat{x}, \hat{y}, \hat{z}$ means that
components parallel (perpendicular) to the $\sharp$ direction are symmetry
allowed, while the others are not allowed. All (**0**) means that all the
components are symmetry allowed (not allowed).

	J_{12}			Y_{12}^x			Y_{12}^y		
G	$\mathbf{D}_{12}$	$\mathbf{E}_{12}$	$\mathbf{F}_{12}$	$\mathbf{A}_{12}^x$	$\mathbf{B}_{12}^x$	$\mathbf{C}_{12}^x$	$\mathbf{A}_{12}^y$	$\mathbf{B}_{12}^y$	$\mathbf{C}_{12}^y$
mmm	**0**	**0**	All	**0**	**0**	**0**	$\parallel \hat{z}$	**0**	**0**
2mm	**0**	**0**	All	**0**	**0**	All	$\parallel \hat{z}$	$\parallel \hat{z}$	**0**
m2m	$\parallel \hat{z}$	**0**	All	**0**	$\parallel \hat{z}$	**0**	$\parallel \hat{z}$	**0**	All
mm2	$\parallel \hat{y}$	**0**	All	**0**	$\parallel \hat{y}$	**0**	$\parallel \hat{z}$	$\parallel \hat{x}$	**0**
222	$\parallel \hat{x}$	**0**	All	**0**	$\parallel \hat{x}$	**0**	$\parallel \hat{z}$	$\parallel \hat{y}$	**0**
2/m..	**0**	$\parallel \hat{x}$	All	$\parallel \hat{x}$	**0**	**0**	$\perp \hat{x}$	**0**	**0**
.2/m.	**0**	$\parallel \hat{y}$	All	$\parallel \hat{y}$	**0**	**0**	$\perp \hat{y}$	**0**	**0**
..2/m	**0**	$\parallel \hat{z}$	All	$\parallel \hat{z}$	**0**	**0**	$\parallel \hat{z}$	**0**	**0**
m..	$\perp \hat{x}$	$\parallel \hat{x}$	All	$\parallel \hat{x}$	$\perp \hat{x}$	**0**	$\perp \hat{x}$	$\parallel \hat{x}$	All
.m.	$\parallel \hat{y}$	$\parallel \hat{y}$	All	$\parallel \hat{y}$	$\parallel \hat{y}$	All	$\perp \hat{y}$	$\perp \hat{y}$	**0**
..m	$\parallel \hat{z}$	$\parallel \hat{z}$	All	$\parallel \hat{z}$	$\parallel \hat{z}$	All	$\parallel \hat{z}$	$\parallel \hat{z}$	All
2..	$\parallel \hat{x}$	$\parallel \hat{x}$	All	$\parallel \hat{x}$	$\parallel \hat{x}$	All	$\perp \hat{x}$	$\perp \hat{x}$	**0**
.2.	$\perp \hat{y}$	$\parallel \hat{y}$	All	$\parallel \hat{y}$	$\perp \hat{y}$	**0**	$\perp \hat{y}$	$\parallel \hat{y}$	All
..2	$\perp \hat{z}$	$\parallel \hat{z}$	All	$\parallel \hat{z}$	$\perp \hat{z}$	**0**	$\parallel \hat{z}$	$\perp \hat{z}$	**0**
$\bar{1}$	**0**	All	All	All	**0**	**0**	All	**0**	**0**
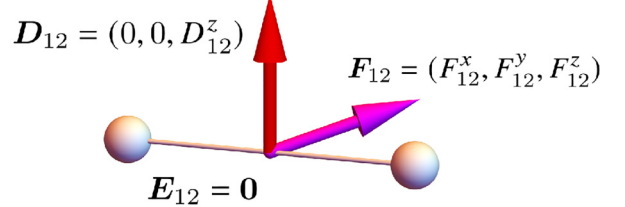
FIG. 1. Model parameters for (a) the $\langle 1, 2 \rangle$ bond with the point
group $m2m$: (b) $\mathbf{D}_{12} = (0, 0, D_{12}^z)$, $\mathbf{E}_{12} = \mathbf{0}$, and $\mathbf{F}_{12}$ in J_{12}, and (c)
$\mathbf{A}_{12}^x = \mathbf{0}$, $\mathbf{B}_{12}^x = (0, 0, B_{12}^{xz})$, $\mathbf{C}_{12}^x = \mathbf{0}$ in Y_{12}^x and $\mathbf{A}_{12}^y = (0, 0, A_{12}^{yz})$,
$\mathbf{B}_{12}^y = \mathbf{0}$, and $\mathbf{C}_{12}^y$ in Y_{12}^y.

interaction originates from the relativistic spin-orbit coupling.
Among them, $\mathbf{D}_{ij}$ is called the DM interaction [21,22].

From the symmetry, the model in Eq. (1) is constructed
once the underlying crystal structure and symmetry of the
bond are given; the form of J_{ij} is determined by the trans-
formation of the $\langle i, j \rangle$ bond. We consider a two-dimensional
system on the xy plane for simplicity, where the bond sym-
metry on the two-dimensional plane is classified into the
orthorhombic point group *mmm* or its subgroups without
two- and three-dimensional irreducible representations. It is
noted that the following result can be extended to a three-
dimensional case. In Table I, we show the constraints on J_{12}
for various point groups $\mathbf{G}$, where the $\langle 1, 2 \rangle$ bond is taken
along the x direction. The symmetry of the $\langle 1, 2 \rangle$ bond is
classified into 15 point groups shown in Table I except for
the point group $\mathbf{G} = 1$, since point group symmetries leaving
the $\langle 1, 2 \rangle$ bond invariant in the one-dimensional irreducible
representation are given by a set of the space inversion (I),
mirror perpendicular to the $\alpha = x, y, z$ axis (m_α), and twofold
rotation around the α axis ($C_{\alpha 2}$). Here, the point group is de-
noted as $\kappa_1 \kappa_2 \kappa_3$ except for $\bar{1}$ with only the inversion symmetry,
where κ_1, κ_2, and κ_3 correspond to either of the symmetry m,
2, $2/m$, or identity "." for the x, y, z axes, respectively; for
example, ..2 (2..) means that the system has twofold rotational
symmetry around the z (x) axis. From Table I, one finds that
the bond with the point group $m2m$ has $\mathbf{D}_{12} = (0, 0, D_{12}^z)$,
$\mathbf{E}_{12} = \mathbf{0}$, and $\mathbf{F}_{12} = (F_{12}^x, F_{12}^y, F_{12}^z)$ owing to m_z, m_x, and C_{y2}
symmetries as an example, as shown in Figs. 1(a) and 1(b).

The correspondence between $\mathbf{G}$ and hexagonal/tetragonal lattice structures is given in Appendix A.

Table I shows that the crystal symmetry imposes constraints on $\boldsymbol{D}_{12}$ and $\boldsymbol{E}_{12}$ but not on $\boldsymbol{F}_{12}$. The main difference between $\boldsymbol{D}_{12}$ and $\boldsymbol{E}_{12}$ is that $\boldsymbol{D}_{12}$ becomes zero but $\boldsymbol{E}_{12}$ is symmetry allowed under the inversion symmetry, as shown in the result for $\mathbf{G} = \bar{1}$. The directions of $\boldsymbol{D}_{12}$ and $\boldsymbol{E}_{12}$ are determined by rotation and mirror symmetries, as shown in the results for $\mathbf{G} = 2..,\,.2.,\,..2,\,m..,\,.m.,$ and $..m$. $\boldsymbol{F}_{12}$ is symmetry allowed for all the point groups, since $S_1^\alpha S_2^\alpha$ is invariant for I, m_β, and $C_{\beta 2}$ ($\beta = x, y, z$). Among the symmetry rules, the rules for the DM interaction is called Moriya's rule [22].

B. Time-dependent Hamiltonian

We take into account effects of an external circularly polarized light on the static model. The model $\mathcal{H}_0$ in Eq. (1) is transformed [24] as

$$\mathcal{H}(t) = \mathcal{H}_0 - \boldsymbol{E}(t) \cdot \boldsymbol{P} - \boldsymbol{B}(t) \cdot \boldsymbol{S}, \tag{3}$$

where the time-dependent electric field $\boldsymbol{E}(t)$ and magnetic field $\boldsymbol{B}(t)$ are coupled with the electric polarization $\boldsymbol{P}$ and the total spin (magnetization) $\boldsymbol{S} = \sum_i \boldsymbol{S}_i$, respectively. We consider the circularly polarized light along the z direction as $\boldsymbol{E}(t) = E_0(\delta \cos \Omega t, -\sin \Omega t, 0)$ and $\boldsymbol{B}(t) = B_0(-\sin \Omega t, -\delta \cos \Omega t, 0)$, where Ω is the light frequency and $\delta = +1(-1)$ represents the right-circularly (left-circularly) polarized light.

In contrast to the magnetization, the expression of the electric polarization depends on the lattice geometry, since it is related to an even order of the spin product. We consider the situation that the electric polarization originates from the spin-dependent electric dipole on the $\langle i, j \rangle$ bond ($i \neq j$) [25,26] as

$$P^\alpha = \sum_{i,j} p_{ij}^\alpha = \sum_{i,j} \sum_{\beta, \gamma} Y_{ij}^{\alpha;\beta\gamma} S_i^\beta S_j^\gamma. \tag{4}$$

Here, the polarization in the whole system is the total of the electric dipole $\boldsymbol{p}_{ij} = (p_{ij}^x, p_{ij}^y, p_{ij}^z)$ at each $\langle i, j \rangle$ bond, where the summation with respect to i, j is taken over the bonds. The $\alpha = x, y, z$ component of the electric dipole is characterized by the third-rank ME tensor $Y_{ij}^{\alpha;\beta\gamma}$, which is given by

$$Y_{ij}^\alpha = \begin{pmatrix} C_{ij}^{\alpha;x} & B_{ij}^{\alpha;z} + A_{ij}^{\alpha;z} & B_{ij}^{\alpha;y} - A_{ij}^{\alpha;y} \\ B_{ij}^{\alpha;z} - A_{ij}^{\alpha;z} & C_{ij}^{\alpha;y} & B_{ij}^{\alpha;x} + A_{ij}^{\alpha;x} \\ B_{ij}^{\alpha;y} + A_{ij}^{\alpha;y} & B_{ij}^{\alpha;x} - A_{ij}^{\alpha;x} & C_{ij}^{\alpha;z} \end{pmatrix}. \tag{5}$$

The third-rank ME tensor consists of antisymmetric off-diagonal components $\boldsymbol{A}_{ij}^\alpha = (A_{ij}^{\alpha;x}, A_{ij}^{\alpha;y}, A_{ij}^{\alpha;z})$, symmetric off-diagonal components $\boldsymbol{B}_{ij}^\alpha = (B_{ij}^{\alpha;x}, B_{ij}^{\alpha;y}, B_{ij}^{\alpha;z})$, and symmetric diagonal components $\boldsymbol{C}_{ij}^\alpha = (C_{ij}^{\alpha;x}, C_{ij}^{\alpha;y}, C_{ij}^{\alpha;z})$, where they satisfy $A_{ij}^\alpha = -A_{ji}^\alpha$, $B_{ij}^\alpha = B_{ji}^\alpha$, and $C_{ij}^\alpha = C_{ji}^\alpha$ with respect to the interchange of two sites. The polarization mechanism for $\boldsymbol{A}_{ij}^\alpha$ is an extension of the inverse DM (spin current) mechanism [27–31], $\boldsymbol{p}_{ij} \propto \boldsymbol{e}_{ij} \times (\boldsymbol{S}_i \times \boldsymbol{S}_j)$ with the bond vector $\boldsymbol{e}_{ij}$. Meanwhile, the mechanism based on the symmetric components $\boldsymbol{C}_{ij}^\alpha$ includes the exchange striction mechanism described by $C_{ij}^{\alpha;x} = C_{ij}^{\alpha;y} = C_{ij}^{\alpha;z}$ [32,33]. Similarly to the coupling matrix J_{ij}, symmetry-allowed components in Y_{ij}^α are determined by the symmetry of the bond, as summarized for Y_{12}^x and Y_{12}^y

under 15 point groups in Table I [34,35]; it is noted that there is no z-directional polarization, i.e., $Y_{12}^z = 0$ owing to $E^z(t) = 0$. In Fig. 1(c), we show the spin-dependent electric dipoles under the $\mathbf{G} = m2m$ symmetry as an example.

The symmetry rules for Y_{12}^x and Y_{12}^y are different from those for J_{12} owing to the different symmetry in the left-hand side in Eqs. (1) and (4); $\mathcal{H}_0$ corresponds to the scalar belonging to the totally symmetric irreducible representation and P^α corresponds to the polar vector belonging to different irreducible representations from $\mathcal{H}_0$. As a result, the inversion symmetry forbids (allows) the antisymmetric components $\boldsymbol{D}_{12}$ (symmetric ones $\boldsymbol{E}_{12}$ and $\boldsymbol{F}_{12}$) in J_{12} and the symmetric ones $\boldsymbol{B}_{12}^\alpha$ and $\boldsymbol{C}_{12}^\alpha$ (antisymmetric one $\boldsymbol{A}_{12}^\alpha$) in Y_{12}^x and Y_{12}^y; see $\mathbf{G} = \bar{1}$ as an example. The directions of $\boldsymbol{A}_{12}^\alpha$, $\boldsymbol{B}_{12}^\alpha$, and $\boldsymbol{C}_{12}^\alpha$ are determined by rotation and mirror symmetries. $A_{12}^{y;z}$ exists for all the point groups, since p_{12}^y and $A_{12}^{y;z}(S_1^x S_2^y - S_2^y S_1^x)$ have the same symmetry. In other words, $A_{12}^{y;z}$ in the third-rank ME tensor is the counterpart of $\boldsymbol{F}_{12}$ in the coupling matrix.

C. Effective time-independent Hamiltonian

We show specific expressions of light-induced anisotropic magnetic interactions in Eq. (3) based on the Floquet theory and the high-frequency expansion [36,37]. The effective Hamiltonian up to the lowest order of Ω^{-1} is given by

$$\mathcal{H}_{\text{eff}} = \mathcal{H}_0 + \frac{1}{\Omega} \sum_{m>0} \frac{[H_{-m}, H_{+m}]}{m}. \tag{6}$$

Here, H_m is the Fourier transform of the time-periodic Hamiltonian, $H(t) = \sum_m e^{-im\Omega t} H_m$ with integer m, and $[H_{-m}, H_{+m}]$ is the commutation relation. Since the light-induced modulation in the second term does not depend on $\mathcal{H}_0$ within the lowest order of Ω^{-1}, the following results are not affected by the original static Hamiltonian. The effective Hamiltonian in Eq. (6) is valid when Ω is larger than the energy scale of the static spin Hamiltonian $\mathcal{H}_0$; Ω is in the terahertz regime since the typical value of the exchange interaction is 0.1–10 meV.

The Fourier transform of the time-periodic Hamiltonian in Eq. (3) is given by

$$H_{+1} = \frac{E_0}{2}(-\delta, i, 0) \cdot \boldsymbol{P} + \frac{B_0}{2}(i, \delta, 0) \cdot \boldsymbol{S}, \tag{7}$$

$$H_{-1} = \frac{E_0}{2}(-\delta, -i, 0) \cdot \boldsymbol{P} + \frac{B_0}{2}(-i, \delta, 0) \cdot \boldsymbol{S}, \tag{8}$$

and $H_{m \neq \pm 1} = 0$. It is noted that Bessel functions do not appear in $H_{\pm 1}$, since we take into account the light effect as the direct coupling to the polarization/magnetization in the localized spin system rather than the Peierls phase of the electron hopping. By substituting H_{+1} and H_{-1} into Eq. (6), the effective Hamiltonian is given by [24]

$$\mathcal{H}_{\text{eff}} = \mathcal{H}_0 + \mathcal{H}_{\text{1spin}} + \mathcal{H}_{\text{2spin}} + \mathcal{H}_{\text{3spin}}, \tag{9}$$

with

$$\mathcal{H}_{\text{1spin}} = -\frac{i\delta B_0^2}{2\Omega}[S^x, S^y] = \frac{\delta B_0^2}{2\Omega} S^z, \tag{10}$$

$$\mathcal{H}_{\text{2spin}} = -\frac{i\delta E_0 B_0}{2\Omega}([P^x, S^x] + [P^y, S^y]), \tag{11}$$

$$\mathcal{H}_{\text{3spin}} = -\frac{i\delta E_0^2}{2\Omega}[P^x, P^y]. \tag{12}$$

$\mathcal{H}_{1\text{spin}}$ corresponds to an effective magnetic field along the z direction coupled with S^z and is irrespective of the third-rank ME tensor; there is no dependence on the crystal structure. It is noted that we use the quantum spin nature in the second equation in Eq. (10). Meanwhile, $\mathcal{H}_{2\text{spin}}$ and $\mathcal{H}_{3\text{spin}}$ lead to two-spin and three-spin interactions, respectively, by calculating the commutation relation, which depend on the third-rank ME tensor including the information about the crystal structure. In other words, $\mathcal{H}_{2\text{spin}}$ and $\mathcal{H}_{3\text{spin}}$ give rise to a variety of light-induced magnetic interactions depending on the crystal symmetry. Indeed, previous studies have shown that the DM interaction is induced in $\mathcal{H}_{2\text{spin}}$ via the inverse DM mechanism [24], a three-spin interaction related to the spin scalar chirality is induced in $\mathcal{H}_{3\text{spin}}$ via the exchange striction mechanism on a honeycomb lattice [23], and a single-ion anisotropy is induced in $\mathcal{H}_{3\text{spin}}$ via the d-p hybridization mechanism [38]. In Sec. III, we present a systematic classification of the light-induced magnetic interactions based on the general third-rank ME tensor that is applicable to any two-dimensional systems.

We estimate a value of the light-induced magnetic interactions by rewriting the coupling between the light and system as $-g\mu_B \boldsymbol{B}_0 \cdot \boldsymbol{S}$ and $-\lambda_{\text{ME}} \boldsymbol{E}_0 \cdot \tilde{\boldsymbol{P}}$ with the g factor g, the Bohr magneton μ_B, the strength of the third-rank ME coupling λ_{ME}, and the dimensionless polarization $\tilde{\boldsymbol{P}}$. With respect to the magnetic-field term, its typical magnitude to the terahertz laser is $B_0 = 1$–10 T. Then, the energy of the coupling to the magnetic field is given by $\epsilon_B = g\mu_B B_0 = 0.1$–$1$ meV. With respect to the electric-field term, λ_{ME} approximately takes a value of 10^{-28}–10^{-26} μCm, where we take 100 Å^3 as the volume of the unit cell, since the polarization in multiferroic materials is typically given by $|\boldsymbol{P}| = 1$–100 μC/m^2 [39]. Then, the energy of the coupling to the electric field is estimated as $\epsilon_E = \lambda_{\text{ME}} E_0 = 0.01$–$0.1$ meV at the most. Thus, both ϵ_B/J and ϵ_E/J range from 0.1–1; the light-induced interactions in Eqs. (10)–(12) are around 0.01–$1 J^2/(2\Omega)$ at the most. The previous study [24] showed that the light-induced $\mathcal{H}_{2\text{spin}}$ with a strength of $0.01J$ is sufficient to modulate the spin texture, and its effects persist for a duration of $400/J$.

Let us comment on details of the light-induced magnetic interactions [24]. First, the magnetic interactions in Eqs. (10)–(12) can be induced even though the light is elliptically polarized, while their amplitudes become smaller than those by the circularly polarized light. It is noted that the magnetic interactions in Eqs. (10)–(12) vanish when linearly polarized light, i.e., $\delta = 0$, is considered. Second, the light-induced magnetic interactions work for a finite time (Floquet prethermal regime), and then they stop modulating magnetic structures. Finally, although the magnetic interactions in Eqs. (10)–(12) are obtained based on the quantum nature of the spin, they can be used to investigate the classical spin dynamics by solving the Landau-Lifshitz-Gilbert (LLG) equation for $\mathcal{H}_{\text{eff}}$ in Eq. (9) with the classical spin [38,40].

In this study, we presume the use of terahertz light in the order of meV in Eq. (6) in the insulating regime with the band gap in the order of eV so that we can ignore a photon absorption and electron excitation. We also presume a negligible spin-lattice (electron-phonon) coupling; we ignore the heating effect. Besides, we do not consider the situation where intense terahertz electric fields (in the order of MV/cm) resonate with an infrared-active phonon mode and induce nonlinear

TABLE II. Change of point group **G**. $\mathcal{H}_{2\text{spin}}$ ($\mathcal{H}_{3\text{spin}}$) changes **G** into the chiral point group **G**$^{(C)}$ (black and white magnetic point group **M**). $\mathcal{H}_{2\text{spin}}$ and $\mathcal{H}_{3\text{spin}}$ change **G** into chiral black and white magnetic point groups **M**$^{(C)}$. The first, second, and third axes are [100], [010], and [001], respectively.

G	**G**$^{(C)}$	**M**	**M**$^{(C)}$
mmm	222	$m'm'm$	$2'2'2$
$2mm$	2..	$2'm'm$	$2'..$
$m2m$	.2.	$m'2'm$	$.2'.$
$mm2$	..2	$m'm'2$	..2
222	222	$2'2'2$	$2'2'2$
$2/m..$	2..	$2'/m'..$	$2'..$
$.2/m.$	.2.	$.2'/m'.$	$.2'.$
$..2/m$	..2	$..2/m$	..2
$m..$	1	$m'..$	1
$.m.$	1	$.m'.$	1
$..m$	1	$..m$	1
2..	2..	$2'..$	$2'..$
.2.	.2.	$.2'.$	$.2'.$
..2	..2	..2	..2
$\bar{1}$	1	$\bar{1}$	1

coupling between infrared-active and Raman phonon modes [41,42], which can result in breaking the crystal symmetry through the spin-lattice (electron-phonon) coupling.

III. SYMMETRY ANALYSIS VIA FLOQUET THEORY

We systematically derive a variety of light-induced magnetic interactions depending on crystal structures: anisotropic two-site two-spin interactions in Sec. III A, anisotropic two-site three-spin interactions in Sec. III B, and anisotropic three-site three-spin interactions in Sec. III C. The former two-spin interaction arises from $\mathcal{H}_{2\text{spin}}$ in Eq. (11), while the latter two types of three-spin interactions arise from $\mathcal{H}_{3\text{spin}}$ in Eq. (12). Our symmetry analysis clarifies that the appearance of the anisotropic two-site two-spin interactions (anisotropic two-site three-spin and three-site three-spin interactions) is due to the reduction of the point group **G** to chiral point group **G**$^{(C)}$ (black and white magnetic point group **M**). We show such a correspondence in Table II.

A. Anisotropic two-site two-spin interaction

First, we show the general expression of the light-induced two-site two-spin interaction that originates from the commutation of the electric polarization $\boldsymbol{P}$ and the magnetization $\boldsymbol{S}$ in Eq. (11). By substituting the third-rank ME tensor in Eq. (5) into Eq. (11), we obtain the light-induced two-site two-spin interaction given by

$$\mathcal{H}_{2\text{spin}} = \sum_{i,j} \sum_{\alpha,\beta} \mathcal{J}_{ij}^{\alpha\beta} S_i^\alpha S_j^\beta, \tag{13}$$

with

$$\mathcal{J}_{ij} = \begin{pmatrix} \mathcal{F}_{ij}^x & \mathcal{E}_{ij}^z + \mathcal{D}_{ij}^z & \mathcal{E}_{ij}^y - \mathcal{D}_{ij}^y \\ \mathcal{E}_{ij}^z - \mathcal{D}_{ij}^z & \mathcal{F}_{ij}^y & \mathcal{E}_{ij}^x + \mathcal{D}_{ij}^x \\ \mathcal{E}_{ij}^y + \mathcal{D}_{ij}^y & \mathcal{E}_{ij}^x - \mathcal{D}_{ij}^x & \mathcal{F}_{ij}^z \end{pmatrix}. \tag{14}$$

Here, the summation is taken over the bonds and spin components; $\mathcal{D}_{ij} = (\mathcal{D}_{ij}^x, \mathcal{D}_{ij}^y, \mathcal{D}_{ij}^z)$ are light-induced DM interactions, $\mathcal{E}_{ij} = (\mathcal{E}_{ij}^x, \mathcal{E}_{ij}^y, \mathcal{E}_{ij}^z)$ are light-induced symmetric off-diagonal interactions, and $\mathcal{F}_{ij} = (\mathcal{F}_{ij}^x, \mathcal{F}_{ij}^y, \mathcal{F}_{ij}^z)$ are light-induced symmetric diagonal interactions. The coupling matrix $\mathcal{J}_{ij}$ is related to the third-rank ME tensor as

$$\frac{2\Omega}{\delta E_0 B_0} \mathcal{D}_{ij}^x = -A_{ij}^{y;z}, \tag{15}$$

$$\frac{2\Omega}{\delta E_0 B_0} \mathcal{D}_{ij}^y = A_{ij}^{x;z}, \tag{16}$$

$$\frac{2\Omega}{\delta E_0 B_0} \mathcal{D}_{ij}^z = -A_{ij}^{x;y} + A_{ij}^{y;x}, \tag{17}$$

$$\frac{2\Omega}{\delta E_0 B_0} \mathcal{E}_{ij}^x = -C_{ij}^{x;y} + C_{ij}^{x;z} + B_{ij}^{y;z}, \tag{18}$$

$$\frac{2\Omega}{\delta E_0 B_0} \mathcal{E}_{ij}^y = -C_{ij}^{y;z} + C_{ij}^{y;x} - B_{ij}^{x;z}, \tag{19}$$

$$\frac{2\Omega}{\delta E_0 B_0} \mathcal{E}_{ij}^z = B_{ij}^{x;y} - B_{ij}^{y;x}, \tag{20}$$

$$\frac{2\Omega}{\delta E_0 B_0} \mathcal{F}_{ij}^x = -2B_{ij}^{y;y}, \tag{21}$$

$$\frac{2\Omega}{\delta E_0 B_0} \mathcal{F}_{ij}^y = 2B_{ij}^{x;x}, \tag{22}$$

$$\frac{2\Omega}{\delta E_0 B_0} \mathcal{F}_{ij}^z = -2B_{ij}^{x;x} + 2B_{ij}^{y;y}, \tag{23}$$

where the antisymmetric (symmetric) interactions are induced by the antisymmetric (symmetric) components in the third-rank ME tensor since the parity with respect to the interchange of two sites in $\mathcal{H}_{2\mathrm{spin}}$ linearly depends on $\boldsymbol{p}_{ij}$. Equations (15)–(23) show that all the types of anisotropic two-site two-spin interactions can be induced by the light depending on the symmetry of the $\langle i, j \rangle$ bond.

To investigate the crystal-structure dependence of the light-induced anisotropic two-site two-spin interaction, we calculate the form of $\mathcal{J}_{12}$ for each point group, as summarized in Table III. These results are obtained by substituting the symmetry-allowed ME components shown in Table I into Eqs. (15)–(23). We find two main characteristics. One is the absence of the light-induced symmetric interactions under point groups with the inversion symmetry, mmm, $2/m..$, $.2/m.$, $..2/m$, and $\bar{1}$, since the symmetric components in the third-rank ME tensor vanish under the inversion symmetry. The other is the presence of the light-induced chiral-type DM interaction $\mathcal{D}_{12}^x$ irrespective of the point group, since $A_{12}^{y;z}$ is symmetry allowed for all the point groups. In other words, the light-induced DM interactions are present irrespective of the inversion symmetry, where they originate from A_{12}^x and A_{12}^y unrelated to the inversion symmetry, as shown in Eqs. (15)–(17) and Table I. From these observations, one can find the opposite tendency of the symmetry-allowed interactions between the light-induced two-site two-spin interaction $\mathcal{J}_{ij}$ and that of the static one J_{ij} in Eq. (1); the inversion symmetry forbids (allows) the static (light-induced) DM interaction, while the inversion symmetry allows (forbids) the static (light-induced) symmetric interaction. This means that

TABLE III. Two-site two-spin interactions $\mathcal{J}_{12}$ under point group **G**. Components with ✓ mean the light-induced ones via Y_{12}^x and Y_{12}^y shown in Table I.

G	$\mathcal{D}_{12}^x$	$\mathcal{D}_{12}^y$	$\mathcal{D}_{12}^z$	$\mathcal{E}_{12}^x$	$\mathcal{E}_{12}^y$	$\mathcal{E}_{12}^z$	$\mathcal{F}_{12}^x$	$\mathcal{F}_{12}^y$	$\mathcal{F}_{12}^z$
mmm	✓								
$2mm$	✓			✓					
$m2m$	✓				✓				
$mm2$	✓					✓			
222	✓						✓	✓	✓
$2/m..$	✓								
$.2/m.$	✓		✓						
$..2/m$	✓	✓							
$m..$	✓				✓	✓			
$.m.$	✓		✓	✓		✓			
$..m$	✓	✓		✓	✓				
$2..$	✓			✓			✓	✓	✓
$.2.$	✓		✓		✓		✓	✓	✓
$..2$	✓	✓				✓	✓	✓	✓
$\bar{1}$	✓	✓	✓						

magnetic structures favored by the static DM interaction in noncentrosymmetric systems, such as a spiral state and skyrmion crystal, can be realized in centrosymmetric systems by applying the circularly polarized light.

There are two effects of light on the two-site two-spin interactions; modification of the static interaction included in J_{12} and induction of new types of interactions not included in J_{12}. By comparing Tables I and III, we find that only the former effect is observed in **G** = 222, 2.., .2., and ..2, while only the latter effect is observed in the other **G** within the lowest-order high-frequency expansion in Eq. (6). The latter interactions result from the symmetry lowering from the original point group by light. It is a different feature from previous studies in the light-driven Mott insulators, where the modification of the static interaction has been focused on [15–20]. As an example of focusing on the latter interaction, it has been shown that the chiral-type DM interaction in the order of Ω^{-3} is induced by irradiating a specific polar metal with the light [43].

We find that the appearance of the light-induced two-site two-spin interactions corresponds to the change of the point group **G** under $\mathcal{H}_{2\mathrm{spin}} \propto i([P^x, S^x] + [P^y, S^y])$. Since $\boldsymbol{P}$ is space-inversion odd and time-reversal even, while $i\boldsymbol{S}$ is space-inversion even and time-reversal even, $\mathcal{H}_{2\mathrm{spin}}$ holds the time-reversal symmetry but breaks the inversion symmetry I. Furthermore, the opposite parity for the mirror symmetry of $\boldsymbol{P}$ and $\boldsymbol{S}$ means the breaking of all the mirror symmetries m_x, m_y, and m_z with keeping all the rotational symmetry C_{x2}, C_{y2}, and C_{z2}. Accordingly, the point group **G** changes into the chiral point group $\mathbf{G}^{(C)}$ by $\mathcal{H}_{2\mathrm{spin}}$ to accommodate the coupling between the polar electric and axial magnetic fields [44]. We show such a symmetry lowering in Table II, where $\mathbf{G}^{(C)}$ is obtained by extracting the symmetries $\{I, m_x, m_y, m_z\}$ from **G**. We confirm that the appearance of the anisotropic two-spin interaction by light based on the perturbation argument is consistent with the reduction to the chiral point groups: When considering the total coupling matrix $J_{12}^{\mathrm{total}} = J_{12} + \mathcal{J}_{12}$,

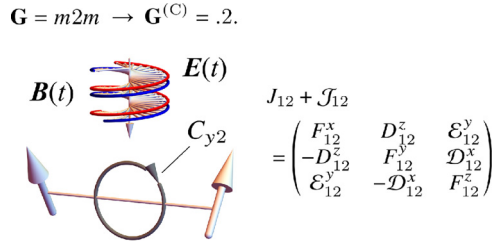$$\mathbf{G} = m2m \rightarrow \mathbf{G}^{(C)} = .2.$$

FIG. 2. The static and light-induced two-site two-spin interactions, where the point group $\mathbf{G} = m2m$ shown in Fig. 1(a) is lowered to the chiral point group $\mathbf{G}^{(C)} = .2.$ by the electric field $\boldsymbol{E}(t)$ (red) and the magnetic field $\boldsymbol{B}(t)$ (blue).

symmetry-allowed components in J_{12}^{total} are determined by the chiral point group $\mathbf{G}^{(C)}$.[1] For example, the point group $m2m$ [Fig. 1(a)] is reduced to the chiral point group $.2.$ (Fig. 2). Then, J_{12}^{total} has light-induced $\mathcal{D}_{12}^x$ and $\mathcal{E}_{12}^y$ in addition to static F_{12} and D_{12}^z, all of which are allowed by $\mathbf{G}^{(C)} = .2.$ (see Table I).

B. Anisotropic two-site three-spin interaction

The anisotropic two-site three-spin interaction is obtained from $\mathcal{H}_{3\text{spin}}$ in Eq. (12) as

$$\mathcal{H}_Q = -\frac{i\delta E_0^2}{2\Omega} \sum_{i,j} [p_{ij}^x, p_{ij}^y]$$
$$= \sum_{i,j} \sum_{\alpha,\beta,\gamma} \{ \mathcal{O}_{ij}^{(S)\alpha\beta\gamma} (Q_i^{\alpha\beta} S_j^\gamma + S_i^\gamma Q_j^{\alpha\beta}) $$
$$+ \mathcal{O}_{ij}^{(AS)\alpha\beta\gamma} (Q_i^{\alpha\beta} S_j^\gamma - S_i^\gamma Q_j^{\alpha\beta}) \}, \quad (24)$$

where the summation is taken over the bonds and spin components; we introduce electric quadrupoles $Q_i^{\alpha\beta}$ at site i, which is defined as

$$Q_i^{\beta\gamma} = \frac{1}{2}(S_i^\beta S_i^\gamma + S_i^\gamma S_i^\beta). \quad (25)$$

Thus, the two-site three-spin interaction is regarded as a spin-quadrupole interaction between two sites. As well as the anisotropic two-site two-spin interaction, the anisotropic two-site three-spin interaction is divided into even and odd components with respect to the interchange of two sites: symmetric ones satisfying $\mathcal{O}_{ij}^{(S)\alpha\gamma} = \mathcal{O}_{ji}^{(S)\alpha\gamma}$ and antisymmetric ones satisfying $\mathcal{O}_{ij}^{(AS)\alpha\gamma} = -\mathcal{O}_{ji}^{(AS)\alpha\gamma}$. In addition, $\mathcal{O}_{ij}^{(S)\alpha\beta\gamma} = \mathcal{O}_{ij}^{(S)\beta\alpha\gamma}$ and $\mathcal{O}_{ij}^{(AS)\alpha\beta\gamma} = \mathcal{O}_{ij}^{(AS)\beta\alpha\gamma}$ hold due to the quadrupole nature.

To derive a general expression of the two-site three-spin interactions in terms of the third-rank ME tensor, we rewrite vectors of the ME couplings as $\tilde{\boldsymbol{A}}_{ij}^\alpha = (A_{ij}^{x;\alpha}, A_{ij}^{y;\alpha}, 0)$, $\tilde{\boldsymbol{B}}_{ij}^\alpha = (B_{ij}^{x;\alpha}, B_{ij}^{y;\alpha}, 0)$, $\tilde{\boldsymbol{C}}_{ij}^\alpha = (C_{ij}^{x;\alpha}, C_{ij}^{y;\alpha}, 0)$ from Eq. (5), where $\tilde{\boldsymbol{A}}_{ij}^\alpha$ ($\tilde{\boldsymbol{B}}_{ij}^\alpha$ and $\tilde{\boldsymbol{C}}_{ij}^\alpha$) is antisymmetric (symmetric) with respect to

the interchange of two sites. Then, the symmetric two-site three-spin interactions are given by

$$\frac{2\Omega}{\delta E_0^2} \mathcal{O}_{ij}^{(S)\alpha\alpha} = \frac{1}{2}\sum_{\beta,\gamma} \epsilon_{\alpha\beta\gamma} (\tilde{\boldsymbol{A}}_{ij}^\beta \times \tilde{\boldsymbol{A}}_{ij}^\gamma - \tilde{\boldsymbol{B}}_{ij}^\beta \times \tilde{\boldsymbol{B}}_{ij}^\gamma)^z, \quad (26)$$

$$\frac{2\Omega}{\delta E_0^2} \mathcal{O}_{ij}^{(S)\alpha\alpha\beta} = -\sum_\gamma \epsilon_{\alpha\beta\gamma} (\tilde{\boldsymbol{C}}_{ij}^\alpha \times \tilde{\boldsymbol{B}}_{ij}^\beta)^z, \quad (27)$$

$$\frac{2\Omega}{\delta E_0^2} \mathcal{O}_{ij}^{(S)\alpha\beta\gamma} = \epsilon_{\alpha\beta\gamma} (\tilde{\boldsymbol{C}}_{ij}^\alpha \times \tilde{\boldsymbol{C}}_{ij}^\beta)^z$$
$$+ \delta_{\alpha\gamma} \sum_\eta \epsilon_{\gamma\beta\eta} (\tilde{\boldsymbol{B}}_{ij}^\eta \times \tilde{\boldsymbol{B}}_{ij}^\gamma$$
$$+ \tilde{\boldsymbol{A}}_{ij}^\eta \times \tilde{\boldsymbol{A}}_{ij}^\gamma + \tilde{\boldsymbol{C}}_{ij}^\beta \times \tilde{\boldsymbol{B}}_{ij}^\beta)^z$$
$$+ \delta_{\beta\gamma} \sum_\eta \epsilon_{\gamma\alpha\eta} (\tilde{\boldsymbol{B}}_{ij}^\eta \times \tilde{\boldsymbol{B}}_{ij}^\gamma$$
$$+ \tilde{\boldsymbol{A}}_{ij}^\eta \times \tilde{\boldsymbol{A}}_{ij}^\gamma + \tilde{\boldsymbol{C}}_{ij}^\alpha \times \tilde{\boldsymbol{B}}_{ij}^\alpha)^z, \quad (28)$$

where $\epsilon_{\alpha\beta\gamma}$ is the Levi-Civita symbol and the z components of the outer product of the vectors originate from $[p_{ij}^x, p_{ij}^y]$. There is no contribution from $\tilde{\boldsymbol{A}}_{ij}^\alpha \times \tilde{\boldsymbol{B}}_{ij}^\beta$ and $\tilde{\boldsymbol{A}}_{ij}^\alpha \times \tilde{\boldsymbol{C}}_{ij}^\beta$, since such products are antisymmetric with respect to the interchange of two sites. By substituting the symmetry-allowed ME components shown in Table I into the general expression, we calculate the symmetric two-site three-spin interactions induced in each point group, as summarized in Table IV.

The product of symmetric and antisymmetric ME components gives rise to the antisymmetric two-site three-spin interactions as

$$\frac{2\Omega}{\delta E_0^2} \mathcal{O}_{ij}^{(AS)\alpha\alpha} = \frac{1}{2}\sum_{\beta,\gamma} |\epsilon_{\alpha\beta\gamma}| (\tilde{\boldsymbol{A}}_{ij}^\beta \times \tilde{\boldsymbol{B}}_{ij}^\gamma + \tilde{\boldsymbol{A}}_{ij}^\gamma \times \tilde{\boldsymbol{B}}_{ij}^\beta)^z, \quad (29)$$

$$\frac{2\Omega}{\delta E_0^2} \mathcal{O}_{ij}^{(AS)\alpha\alpha\beta} = (1 - \delta_{\alpha\beta})(\tilde{\boldsymbol{C}}_{ij}^\alpha \times \tilde{\boldsymbol{A}}_{ij}^\beta)^z, \quad (30)$$

$$\frac{2\Omega}{\delta E_0^2} \mathcal{O}_{ij}^{(AS)\alpha\beta\gamma} = 2|\epsilon_{\alpha\beta\gamma}| (\tilde{\boldsymbol{B}}_{ij}^\gamma \times \tilde{\boldsymbol{A}}_{ij}^\gamma)^z$$
$$+ \delta_{\alpha\gamma} \sum_\eta |\epsilon_{\gamma\beta\eta}| (\tilde{\boldsymbol{B}}_{ij}^\eta \times \tilde{\boldsymbol{A}}_{ij}^\gamma$$
$$+ \tilde{\boldsymbol{A}}_{ij}^\eta \times \tilde{\boldsymbol{B}}_{ij}^\gamma - \tilde{\boldsymbol{C}}_{ij}^\beta \times \tilde{\boldsymbol{A}}_{ij}^\beta)^z$$
$$+ \delta_{\beta\gamma} \sum_\eta |\epsilon_{\gamma\alpha\eta}| (\tilde{\boldsymbol{B}}_{ij}^\eta \times \tilde{\boldsymbol{A}}_{ij}^\gamma$$
$$+ \tilde{\boldsymbol{A}}_{ij}^\eta \times \tilde{\boldsymbol{B}}_{ij}^\gamma - \tilde{\boldsymbol{C}}_{ij}^\alpha \times \tilde{\boldsymbol{A}}_{ij}^\alpha)^z. \quad (31)$$

These general expressions mean that the antisymmetric two-site three-spin interactions vanish on the inversion-symmetric bond, where all the symmetric ME components are zero, as discussed in Sec. II A. The antisymmetric two-site three-spin interactions induced in each point group are shown in Table V.

---

[1] When the point groups do not have symmetries $\{I, m_x, m_y, m_z\}$ in $\mathbf{G}$, such as 222, 2.., .2., and ..2, no symmetry reduction occurs; no additional two-spin interaction appears but the static two-spin interactions are modulated.

[2] When the point groups do not have symmetries $\{m_x, m_y, C_{2x}, C_{2y}\}$ in $\mathbf{G}$, such as ..2/m, ..m, .2., and $\bar{1}$, no symmetry reduction to the black and white magnetic point group occurs; the three-spin interactions appear through the breaking of the time-reversal symmetry.

TABLE IV. Symmetric two-site three-spin interactions $\mathcal{O}_{12}^{(S)}$ under point group **G**. Components listed here are induced by the light through (Y_{12}^x, Y_{12}^y) shown in Table I.

G	$\mathcal{O}_{12}^{(S)\alpha\beta x}$	$\mathcal{O}_{12}^{(S)\alpha\beta y}$	$\mathcal{O}_{12}^{(S)\alpha\beta z}$
mmm			
$2mm$	$\mathcal{O}_{12}^{(S)zxx}$	$\mathcal{O}_{12}^{(S)yzy}$	$\mathcal{O}_{12}^{(S)xxz}, \mathcal{O}_{12}^{(S)yyz}$
$m2m$	$\mathcal{O}_{12}^{(S)zxx}$	$\mathcal{O}_{12}^{(S)yzy}$	$\mathcal{O}_{12}^{(S)xxz}, \mathcal{O}_{12}^{(S)yyz}$
$mm2$	$\mathcal{O}_{12}^{(S)zxx}$	$\mathcal{O}_{12}^{(S)yzy}$	$\mathcal{O}_{12}^{(S)zzz}$
222	$\mathcal{O}_{12}^{(S)zxx}$	$\mathcal{O}_{12}^{(S)yzy}$	$\mathcal{O}_{12}^{(S)zzz}$
$2/m..$	$\mathcal{O}_{12}^{(S)xyx}, \mathcal{O}_{12}^{(S)zxx}$	$\mathcal{O}_{12}^{(S)yyy}, \mathcal{O}_{12}^{(S)yzy}$	$\mathcal{O}_{12}^{(S)zzz}, \mathcal{O}_{12}^{(S)yzz}$
$.2/m.$	$\mathcal{O}_{12}^{(S)xxx}, \mathcal{O}_{12}^{(S)zxx}$	$\mathcal{O}_{12}^{(S)yzy}, \mathcal{O}_{12}^{(S)xyy}$	$\mathcal{O}_{12}^{(S)zzz}, \mathcal{O}_{12}^{(S)zxz}$
$..2/m$			
$m..$	$\mathcal{O}_{12}^{(S)xyx}, \mathcal{O}_{12}^{(S)zxx}$	$\mathcal{O}_{12}^{(S)xxy}, \mathcal{O}_{12}^{(S)zzy} \mathcal{O}_{12}^{(S)yyy}, \mathcal{O}_{12}^{(S)yzy}$	$\mathcal{O}_{12}^{(S)xxz}, \mathcal{O}_{12}^{(S)yyz}, \mathcal{O}_{12}^{(S)zzz}, \mathcal{O}_{12}^{(S)yzz}$
$.m.$	$\mathcal{O}_{12}^{(S)xxx}, \mathcal{O}_{12}^{(S)yyx}, \mathcal{O}_{12}^{(S)zzx}, \mathcal{O}_{12}^{(S)zxx}$	$\mathcal{O}_{12}^{(S)yzy}, \mathcal{O}_{12}^{(S)xyy}$	$\mathcal{O}_{12}^{(S)xxz}, \mathcal{O}_{12}^{(S)yyz}, \mathcal{O}_{12}^{(S)zzz}, \mathcal{O}_{12}^{(S)zxz}$
$..m$	$\mathcal{O}_{12}^{(S)yzx}, \mathcal{O}_{12}^{(S)zxx}$	$\mathcal{O}_{12}^{(S)yzy}, \mathcal{O}_{12}^{(S)zxy}$	$\mathcal{O}_{12}^{(S)xxz}, \mathcal{O}_{12}^{(S)yyz}, \mathcal{O}_{12}^{(S)xyz}$
$2..$	$\mathcal{O}_{12}^{(S)xyx}, \mathcal{O}_{12}^{(S)zxx}$	$\mathcal{O}_{12}^{(S)xxy}, \mathcal{O}_{12}^{(S)zzy} \mathcal{O}_{12}^{(S)yyy}, \mathcal{O}_{12}^{(S)yzy}$	$\mathcal{O}_{12}^{(S)xxz}, \mathcal{O}_{12}^{(S)yyz}, \mathcal{O}_{12}^{(S)zzz}, \mathcal{O}_{12}^{(S)yzz}$
$.2.$	$\mathcal{O}_{12}^{(S)xxx}, \mathcal{O}_{12}^{(S)yyx}, \mathcal{O}_{12}^{(S)zzx}, \mathcal{O}_{12}^{(S)zxx}$	$\mathcal{O}_{12}^{(S)yzy}, \mathcal{O}_{12}^{(S)xyy}$	$\mathcal{O}_{12}^{(S)xxz}, \mathcal{O}_{12}^{(S)yyz}, \mathcal{O}_{12}^{(S)zzz}, \mathcal{O}_{12}^{(S)zxz}$
$..2$	$\mathcal{O}_{12}^{(S)zxx}$	$\mathcal{O}_{12}^{(S)yzy}$	$\mathcal{O}_{12}^{(S)zzz}$
$\bar{1}$	$\mathcal{O}_{12}^{(S)xxx}, \mathcal{O}_{12}^{(S)xyx}, \mathcal{O}_{12}^{(S)zxx}$	$\mathcal{O}_{12}^{(S)yyy}, \mathcal{O}_{12}^{(S)xyy}, \mathcal{O}_{12}^{(S)yzy}$	$\mathcal{O}_{12}^{(S)zzz}, \mathcal{O}_{12}^{(S)yzz}, \mathcal{O}_{12}^{(S)zxz}$

To understand the light-induced two-site three-spin interactions based on the crystal symmetry, we investigate symmetry reduction from the point group **G** under $\mathcal{H}_{3\mathrm{spin}}$. As shown in Eq. (12), $\mathcal{H}_{3\mathrm{spin}}$ is proportional to $i[P^x, P^y]$, which has the same symmetry with the magnetization along the z direction. The z magnetization breaks the point group symmetries $\{m_x, m_y, C_{2x}, C_{2y}\}$ but holds these point group symmetries combined with the time-reversal symmetry denoted as $\{m'_x, m'_y, C'_{2x}, C'_{2y}\}$. Thus, $\mathcal{H}_{3\mathrm{spin}}$ changes the point group **G** into the black and white magnetic point group **M** [45], as shown in Table II; **M** and **G** in Table II are related as $\mathbf{M} = (\mathbf{G} - \bar{\mathbf{G}}) + \theta\bar{\mathbf{G}}$, where $\bar{\mathbf{G}} = \mathbf{G} \cap \{m_x, m_y, C_{2x}, C_{2y}\}$ and θ is the time-reversal operation.[2] We show a symmetry rule for the two-site three-spin interactions in Table VI and confirm that the induced interactions in Tables IV and V satisfy the symmetry rule. For example, the point group $m2m$ [Fig. 1(a)] is reduced to the black and white magnetic point group $m'2'm$ (Fig. 3), and $\mathcal{O}_{12}^{(S)zxx}$, $\mathcal{O}_{12}^{(S)yzy}$, $\mathcal{O}_{12}^{(S)xxz}$, $\mathcal{O}_{12}^{(S)yyz}$, and $\mathcal{O}_{12}^{(AS)xyz}$ are

TABLE V. Antisymmetric two-site three-spin interactions $\mathcal{O}_{12}^{(AS)}$ under point group **G**. Components listed here are induced by the light through (Y_{12}^x, Y_{12}^y) shown in Table I.

G	$\mathcal{O}_{12}^{(AS)\alpha\beta x}$	$\mathcal{O}_{12}^{(AS)\alpha\beta y}$	$\mathcal{O}_{12}^{(AS)\alpha\beta z}$
mmm			
$2mm$	$\mathcal{O}_{12}^{(AS)zxx}$	$\mathcal{O}_{12}^{(AS)yzy}$	$\mathcal{O}_{12}^{(AS)xxz}, \mathcal{O}_{12}^{(AS)yyz}$
$m2m$			$\mathcal{O}_{12}^{(AS)xyz}$
$mm2$	$\mathcal{O}_{12}^{(AS)xxx}$	$\mathcal{O}_{12}^{(AS)xyy}$	$\mathcal{O}_{12}^{(AS)zxz}$
222	$\mathcal{O}_{12}^{(AS)xyx}$	$\mathcal{O}_{12}^{(AS)yyy}$	$\mathcal{O}_{12}^{(AS)yzz}$
$2/m..$			
$.2/m.$			
$..2/m$			
$m..$	$\mathcal{O}_{12}^{(AS)xxx}, \mathcal{O}_{12}^{(AS)yyx}, \mathcal{O}_{12}^{(AS)zzx}, \mathcal{O}_{12}^{(AS)yzx}$	$\mathcal{O}_{12}^{(AS)xyy},$	$\mathcal{O}_{12}^{(AS)xyz}, \mathcal{O}_{12}^{(AS)zxz}$
$.m.$	$\mathcal{O}_{12}^{(AS)xxx}, \mathcal{O}_{12}^{(AS)yyx}, \mathcal{O}_{12}^{(AS)zzx}, \mathcal{O}_{12}^{(AS)zxx}$	$\mathcal{O}_{12}^{(AS)xyy}, \mathcal{O}_{12}^{(AS)yzy}$	$\mathcal{O}_{12}^{(AS)xxz}, \mathcal{O}_{12}^{(AS)yyz}, \mathcal{O}_{12}^{(AS)zzz}, \mathcal{O}_{12}^{(AS)zxz}$
$..m$	$\mathcal{O}_{12}^{(AS)zxx}$	$\mathcal{O}_{12}^{(AS)yzy}$	$\mathcal{O}_{12}^{(AS)xxz}, \mathcal{O}_{12}^{(AS)yyz}, \mathcal{O}_{12}^{(AS)xyz}$
$2..$	$\mathcal{O}_{12}^{(AS)xyx}, \mathcal{O}_{12}^{(AS)zxx}$	$\mathcal{O}_{12}^{(AS)xxy}, \mathcal{O}_{12}^{(AS)yyy}, \mathcal{O}_{12}^{(AS)zzy}, \mathcal{O}_{12}^{(AS)yzy}$	$\mathcal{O}_{12}^{(AS)xxz}, \mathcal{O}_{12}^{(AS)yyz}, \mathcal{O}_{12}^{(AS)zzz}, \mathcal{O}_{12}^{(AS)yzz}$
$.2.$	$\mathcal{O}_{12}^{(AS)xyx}, \mathcal{O}_{12}^{(AS)yzx}$	$\mathcal{O}_{12}^{(AS)xxy}, \mathcal{O}_{12}^{(AS)yyy}, \mathcal{O}_{12}^{(AS)zzy}, \mathcal{O}_{12}^{(AS)zxy}$	$\mathcal{O}_{12}^{(AS)xyz}, \mathcal{O}_{12}^{(AS)yzz}$
$..2$	$\mathcal{O}_{12}^{(AS)xxx} \mathcal{O}_{12}^{(AS)xyx}$	$\mathcal{O}_{12}^{(AS)yyy}, \mathcal{O}_{12}^{(AS)xyy}$	$\mathcal{O}_{12}^{(AS)yzz}, \mathcal{O}_{12}^{(AS)zxz}$
$\bar{1}$			

TABLE VI. Symmetry rules of the two-site three-spin interactions: $\{\mathcal{O}_{12}^{(S/AS)xxx}\} = \{\mathcal{O}_{12}^{(S/AS)xxx}, \mathcal{O}_{12}^{(S/AS)yyx}, \mathcal{O}_{12}^{(S/AS)zzx}, \mathcal{O}_{12}^{(S/AS)xyy}, \mathcal{O}_{12}^{(S/AS)zxz}\}$, $\{\mathcal{O}_{12}^{(S/AS)yyy}\} = \{\mathcal{O}_{12}^{(S/AS)xyx}, \mathcal{O}_{12}^{(S/AS)xxy}, \mathcal{O}_{12}^{(S/AS)yyy}, \mathcal{O}_{12}^{(S/AS)zzy}, \mathcal{O}_{12}^{(S/AS)yzz}\}$, $\{\mathcal{O}_{12}^{(S/AS)zzz}\} = \{\mathcal{O}_{12}^{(S/AS)zxx}, \mathcal{O}_{12}^{(S/AS)yzy}, \mathcal{O}_{12}^{(S/AS)xxz}, \mathcal{O}_{12}^{(S/AS)yyz}, \mathcal{O}_{12}^{(S/AS)zzz}\}$, and $\{\mathcal{O}_{12}^{(S/AS)xyz}\} = \{\mathcal{O}_{12}^{(S/AS)yzx}, \mathcal{O}_{12}^{(S/AS)zxy}, \mathcal{O}_{12}^{(S/AS)xyz}\}$. All (0) means that all the components in $\{\cdots\}$ are symmetry allowed (not allowed).

M	$\{\mathcal{O}_{12}^{(S)xxx}\}$	$\{\mathcal{O}_{12}^{(S)yyy}\}$	$\{\mathcal{O}_{12}^{(S)zzz}\}$	$\{\mathcal{O}_{12}^{(S)xyz}\}$	$\{\mathcal{O}_{12}^{(AS)xxx}\}$	$\{\mathcal{O}_{12}^{(AS)yyy}\}$	$\{\mathcal{O}_{12}^{(AS)zzz}\}$	$\{\mathcal{O}_{12}^{(AS)xyz}\}$
$m'm'm$	0	0	All	0	0	0	0	0
$2'm'm$	0	0	All	0	0	0	All	0
$m'2'm$	0	0	All	0	0	0	0	All
$m'm'2$	0	0	All	0	All	0	0	0
$2'2'2$	0	0	All	0	0	All	0	0
$2'/m'..$	0	All	All	0	0	0	0	0
$.2'/m'.$	All	0	All	0	0	0	0	0
$..2/m$	0	0	All	All	0	0	0	0
$m'..$	0	All	All	0	All	0	0	All
$.m'.$	All	0	All	0	All	0	All	0
$..m$	0	0	All	All	0	0	All	All
$2'..$	0	All	All	0	0	All	All	0
$.2'.$	All	0	All	0	0	All	0	All
$..2$	0	0	All	All	All	All	0	0
$\bar{1}$	All	All	All	All	0	0	0	0

induced, where the symmetry-allowed $\mathcal{O}_{12}^{(S)zzz}$ is not induced in the present perturbation process.

Although the above results can be applied to spin systems with any spin length, it is noted in the case of a spin-half system; the electric quadrupole in Eq. (25) is given by $Q_i^{\alpha\beta} = \delta_{\alpha\beta}/4$. Then, the interaction in Eq. (24) becomes

$$\mathcal{H}_Q = \frac{1}{4}\sum_{\langle i,j\rangle}\sum_{\alpha,\gamma}\left\{\mathcal{O}_{ij}^{(S)\alpha\alpha\gamma}\left(S_j^\gamma + S_i^\gamma\right) + \mathcal{O}_{ij}^{(AS)\alpha\alpha\gamma}\left(S_j^\gamma - S_i^\gamma\right)\right\},$$
(32)

where the first (second) term corresponds to a uniform (staggered) magnetic field for two spins.

C. Anisotropic three-site three-spin interaction

The three-site three-spin interaction is obtained from the commutation relation between the electric dipoles at different

$$\mathbf{G} = m2m \;\rightarrow\; \mathbf{M} = m'2'm$$

$E(t)$

C'_{y2}

m_z

m'_x

$O_{12}^{(S)zxx}, O_{12}^{(S)yzy},$
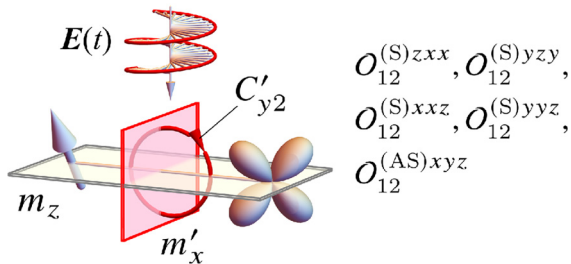$O_{12}^{(S)xxz}, O_{12}^{(S)yyz},$
$O_{12}^{(AS)xyz}$

FIG. 3. The light-induced two-site three-spin interactions, where the reduction from the point group $\mathbf{G} = m2m$ shown in Fig. 1(a) to the black and white magnetic point group $\mathbf{M} = m'2'm$ occurs by the electric field $\boldsymbol{E}(t)$.

sites in $\mathcal{H}_{3\text{spin}}$ in Eq. (12) as

$$\mathcal{H}_{3\text{site}} = -\frac{i\delta E_0^2}{2\Omega}\sum_j\sum_{i\neq k}\left([p_{ij}^x, p_{jk}^y] + [p_{jk}^x, p_{ij}^y]\right)$$

$$= \frac{\delta E_0^2}{2\Omega}\sum_j\sum_{i\neq k}\sum_{\alpha,\beta,\gamma,\zeta,\eta}\epsilon_{\beta\gamma\eta}$$

$$\times \left(Y_{ij}^{x;\alpha\beta}Y_{jk}^{y;\gamma\zeta} - Y_{ij}^{y;\alpha\beta}Y_{jk}^{x;\gamma\zeta}\right)S_i^\alpha S_j^\eta S_k^\zeta.$$
(33)

Similarly to the anisotropic two-site two-spin and two-site three-spin interactions, the form of the three-site three-spin interaction is determined by the crystal symmetry via the third-rank ME tensor. Meanwhile, the symmetry conditions between them are different from each other: The anisotropic two-site two-spin and two-site three-spin interactions depend on the symmetry of the bond, while the three-site three-spin interactions depend on the symmetry of the plaquette consisting of the sites i, j, and k. Thus, the presence of the three-site three-spin interactions depends on the relative positions of the sites i, j, and k, which indicates that they are not simply classified by the point groups in Table I. From the symmetry viewpoint, the emergence of the three-site three-spin interactions is explained by the change of the symmetry of the plaquette into the black and white magnetic point group, as shown in Sec. IV B 4.

IV. APPLICATION TO A TRIANGULAR UNIT

We apply the above results to a triangular unit with the point group $m2\bar{6}$ shown in Fig. 4. By starting from a static Hamiltonian in Sec. IV A, we show the light-induced one-spin, anisotropic two-site two-spin, anisotropic two-site three-spin, anisotropic three-site three-spin interactions in Secs. IV B 1–IV B 4, respectively. In each case, we discuss the modulation of a spin structure under the light-induced anisotropic interactions by taking the classical spin limit for simplicity.
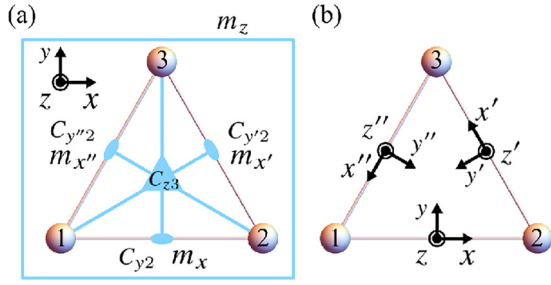
FIG. 4. (a) Triangular unit under the point group $m2\bar{6}$. (b) Local Cartesian spin coordinates (x, y, z) for the $\langle 1, 2 \rangle$ bond, (x', y', z') for the $\langle 2, 3 \rangle$ bond, and (x'', y'', z'') for the $\langle 3, 1 \rangle$ bond.

A. Static Hamiltonian

We start from the static Hamiltonian in Eq. (1) in the $m2\bar{6}$ triangular unit, which is given by

$$
\mathcal{H}_0 = \sum_{\alpha,\beta} \left(J_{12}^{\alpha\beta} S_1^\alpha S_2^\beta + J_{23}^{\alpha\beta} S_2^\alpha S_3^\beta + J_{31}^{\alpha\beta} S_3^\alpha S_1^\beta \right)
$$

$$
= \sum_{\alpha,\beta} J_{12}^{\alpha\beta} \left(S_1^\alpha S_2^\beta + S_2^{\alpha'} S_3^{\beta'} + S_3^{\alpha''} S_1^{\beta''} \right). \tag{34}
$$

The Hamiltonian in the first line is written in the global Cartesian spin coordinate $\mathbf{S} = (S^x, S^y, S^z)$. We fix the spin length $|\mathbf{S}_i| = 1$ in each site for simplicity. The coupling matrices $J_{23}^{\alpha\beta}$, and $J_{31}^{\alpha\beta}$ are related to $J_{12}^{\alpha\beta}$ due to the threefold rotation around the z axis. By using the local Cartesian spin coordinates $\mathbf{S}$ for the $\langle 1, 2 \rangle$ bond, $\mathbf{S}' = (S^x, S^{y'}, S^z)$ for the $\langle 2, 3 \rangle$ bond, and $\mathbf{S}'' = (S^{x''}, S^{y''}, S^{z''})$ for the $\langle 3, 1 \rangle$ bond shown in Fig. 4(b), the Hamiltonian is represented by the second line. Thus, the Hamiltonian is characterized by J_{12}, which is given by

$$
J_{12} = \begin{pmatrix} F^x & D^z & 0 \\ -D^z & F^y & 0 \\ 0 & 0 & F^z \end{pmatrix}. \tag{35}
$$

The form of J_{12} is determined by the point group $m2m$ of the $\langle 1, 2 \rangle$ bond (see also Table I). $J_{23}^{\alpha\beta}$ and $J_{31}^{\alpha\beta}$ written in the global Cartesian spin coordinate are shown in Appendix B.

We discuss the ground-state spin configuration in $\mathcal{H}_0$ by using the irreducible representation Γ under the point group $m2\bar{6}$: $\Gamma = A_1', A_2', A_1'', A_2'', E', $ and E'' shown in Table VII. The arbitrary spin configuration $S^\triangle = (\mathbf{S}_1, \mathbf{S}_2, \mathbf{S}_3)$ is expressed by

TABLE VII. Irreducible representations and character table for the point group $m2\bar{6}$.

	E	m_z	$2C_{z3}$	$2S_6$	$3C_{y2}$	$3m_x$
A_1'	1	1	1	1	1	1
A_2'	1	1	1	1	-1	-1
A_1''	1	-1	1	-1	1	-1
A_2''	1	-1	1	-1	-1	1
E'	2	2	-1	-1	0	0
E''	2	-2	-1	1	0	0
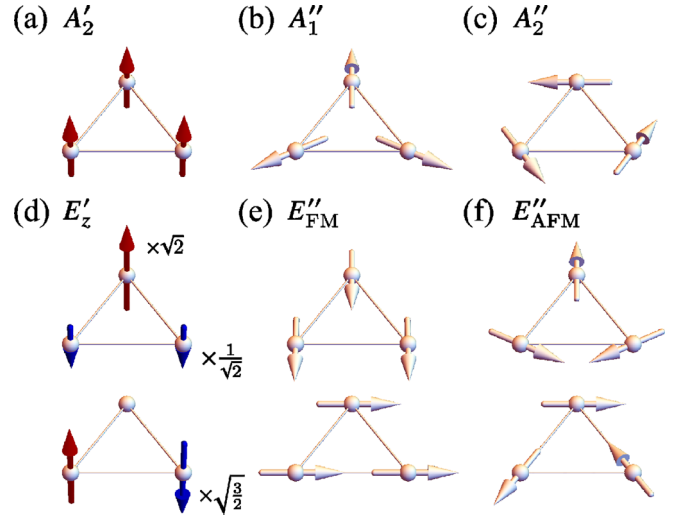
FIG. 5. Bases for the irreducible representations (a) A_2', (b) A_1'', (c) A_2'', (d) E_z', (e) E_{FM}'', and (f) E_{AFM}''. Top and bottom panels in two-dimensional representations [(d)–(f)] correspond to the bases with the same representation matrix as that for x and y, respectively. The color shows the z spin components, where red, white, and blue correspond to the positive, zero, and negative ones, respectively. The spin length at each site is fixed as $|\mathbf{S}_i| = 1$ except for (d): $(|\mathbf{S}_1|, |\mathbf{S}_2|, |\mathbf{S}_3|) = (1/\sqrt{2}, 1/\sqrt{2}, \sqrt{2})$ for the top panel in (d) and $(|\mathbf{S}_1|, |\mathbf{S}_2|, |\mathbf{S}_3|) = (\sqrt{3/2}, \sqrt{3/2}, 0)$ for the bottom panel in (d). The details of the spin configurations are shown in Appendix C.

bases $S(\Gamma)$ for the irreducible representation Γ as

$$
S^\triangle = m_{A_2'} S(A_2') + m_{A_1''} S(A_1'') + m_{A_2''} S(A_2'')
$$
$$
+ \mathbf{m}_{E_z'} \cdot \mathbf{S}(E_z') + \mathbf{m}_{E_{\text{FM}}''} \cdot \mathbf{S}(E_{\text{FM}}'')
$$
$$
+ \mathbf{m}_{E_{\text{AFM}}''} \cdot \mathbf{S}(E_{\text{AFM}}''), \tag{36}
$$

where $S(\Gamma)$ is the nine-dimensional vector, whose components are given by the spin configurations shown in Fig. 5, and m_Γ is the order parameter of $S(\Gamma)$. We use $\mathbf{S}(\Gamma) = (S_\Gamma^x, S_\Gamma^y)$ and $\mathbf{m}_\Gamma = (m_\Gamma^x, m_\Gamma^y)$ for the two-dimensional representations. By using Eq. (36), the Hamiltonian in Eq. (34) is rewritten as

$$
\mathcal{H}_0 = \frac{3}{2} \left(\lambda_{A_2'} m_{A_2'}^2 + \lambda_{A_1''} m_{A_1''}^2 + \lambda_{A_2''} m_{A_2''}^2 \right.
$$
$$
+ \lambda_{E_z'} \mathbf{m}_{E_z'}^2 + \lambda_{E_{\text{FM}}''} \mathbf{m}_{E_{\text{FM}}''}^2 + \lambda_{E_{\text{AFM}}''} \mathbf{m}_{E_{\text{AFM}}''}^2
$$
$$
\left. + \lambda_{E''} \mathbf{m}_{E_{\text{FM}}''} \cdot \mathbf{m}_{E_{\text{AFM}}''} \right), \tag{37}
$$

with

$$
\lambda_{A_2'} = 2F^z, \tag{38}
$$

$$
\lambda_{A_1''} = \frac{1}{2}(-3F^x + F^y + 2\sqrt{3}D^z), \tag{39}
$$

$$
\lambda_{A_2''} = \frac{1}{2}(F^x - 3F^y + 2\sqrt{3}D^z), \tag{40}
$$

$$
\lambda_{E_z'} = -F^z, \tag{41}
$$

$$
\lambda_{E_{\text{FM}}''} = F^x + F^y, \tag{42}
$$

$$
\lambda_{E_{\text{AFM}}''} = \frac{1}{2}(-F^x - F^y - 2\sqrt{3}D^z), \tag{43}
$$

$$
\lambda_{E''} = -F^x + F^y. \tag{44}
$$

The ground-state spin configuration in the classical spin limit is obtained as follows. Due to constraint on the spin length at each site ($|\mathbf{S}_i| = 1$), the order parameters satisfy $|m_\Gamma^\alpha| \leqslant 1$ and $\sum_{\alpha,\Gamma}(m_\Gamma^\alpha)^2 = 1$. Then, the ground-state spin configuration is given by $S^\triangle$ with $|m_{\Gamma_{\min}}| = 1$ and $m_{\Gamma \neq \Gamma_{\min}} = 0$, where the state with $\Gamma_{\min}$ gives the smallest eigenvalue $\lambda_{\Gamma_{\min}}$. Various spin configurations become the ground state depending on the model parameters in J_{12} [46], while all of them are collinear, $S(A_2')$, $S(E_z')$, and $S(E_{\mathrm{FM}}'')$, or coplanar, $S(A_1'')$, $S(A_2'')$, and $S(E_{\mathrm{AFM}}'')$. This is because the coupling matrix J_{12} has no components mixing the z and xy spins, such as J_{12}^{yz} and J_{12}^{zx}, due to the horizontal mirror symmetry m_z.

B. Light-induced magnetic interactions

We show the light-induced magnetic interactions in the triangular unit and discuss a modulation of the spin configuration in the classical spin limit. The third-rank ME tensor on the $\langle 1, 2 \rangle$ bond is given by

$$Y_{12}^x = \begin{pmatrix} 0 & B_{12}^{x;z} & 0 \\ B_{12}^{x;z} & 0 & 0 \\ 0 & 0 & 0 \end{pmatrix}, \tag{45}$$

$$Y_{12}^y = \begin{pmatrix} C_{12}^{y;x} & A_{12}^{y;z} & 0 \\ -A_{12}^{y;z} & C_{12}^{y;y} & 0 \\ 0 & 0 & C_{12}^{y;z} \end{pmatrix}. \tag{46}$$

Here, symmetry-allowed components are determined by the point group symmetry $m2m$ of the $\langle 1, 2 \rangle$ bond, as shown in Table I. The third-rank ME tensors on the other bonds are given by components in (Y_{12}^x, Y_{12}^y) via the threefold rotation, as shown in Appendix B.

1. $\mathcal{H}_{1\mathrm{spin}}$

The light-induced one-spin term is given by

$$\begin{aligned} \mathcal{H}_{1\mathrm{spin}} &= \frac{\delta B_0^2}{2\Omega}\left(S_1^z + S_2^z + S_3^z\right) \\ &= \frac{3\delta B_0^2}{2\Omega} m_{A_2'}. \end{aligned} \tag{47}$$

Thus, $\mathcal{H}_{1\mathrm{spin}}$ favors $S^\triangle = m_{A_2'}S(A_2')$ with $m_{A_2'} = -1$ ($m_{A_2'} = +1$) for the right-circularly (left-circularly) polarized light with $\delta = +1$ ($\delta = -1$).

2. $\mathcal{H}_{2\mathrm{spin}}$

In $\mathcal{H}_{2\mathrm{spin}}$, we obtain the light-induced DM interaction $\mathcal{H}_{2\mathrm{spin}}^{(1)}$ with $\mathcal{D}_{12}^x$ and the light-induced symmetric off-diagonal interaction $\mathcal{H}_{2\mathrm{spin}}^{(2)}$ with $\mathcal{E}_{12}^y$. Here, $\mathcal{D}_{12}^x$ and $\mathcal{E}_{12}^y$ are allowed by the chiral point group $\mathbf{G}^{(C)} = .2.$ of the $\langle 1, 2 \rangle$ bond. Reflecting the threefold rotation, the symmetry-equivalent interactions are induced by the light on the $\langle 2, 3 \rangle$ and $\langle 3, 1 \rangle$ bonds.

The light-induced DM interaction is given by

$$\begin{aligned} \mathcal{H}_{2\mathrm{spin}}^{(1)} &= \mathcal{D}_{12}^x(\mathbf{S}_1 \times \mathbf{S}_2 + \mathbf{S}_2' \times \mathbf{S}_3' + \mathbf{S}_3'' \times \mathbf{S}_1'')^x \\ &= -3\sqrt{3}\mathcal{D}_{12}^x\left[m_{A_2'}m_{A_2''} + \frac{1}{\sqrt{2}}(\mathbf{m}_{E_z'} \times \mathbf{m}_{E_{\mathrm{FM}}''})^z\right], \end{aligned} \tag{48}$$

where $\mathcal{D}_{12}^x = -\delta E_0 B_0 A_{12}^{y;z}/2\Omega$. From the second line, we find that the DM interaction is represented by a linear combination of the terms belonging to A_1'' owing to the breaking of the mirror symmetries $\{m_x, m_y, m_z\}$ by the light. In other words, the light-induced DM interaction belongs to the totally symmetric irreducible representation of the chiral point group $\mathbf{G}^{(C)} = .23$ of the triangle unit. In the classical spin limit, the DM interaction favors

$$S^\triangle = m_{A_2'}S(A_2') + m_{A_2''}S(A_2''), \tag{49}$$

with $m_{A_2'} = m_{A_2''} = \pm\frac{1}{\sqrt{2}}$ for $\mathcal{D}_{12}^x > 0$ and $m_{A_2'} = -m_{A_2''} = \pm\frac{1}{\sqrt{2}}$ for $\mathcal{D}_{12}^x < 0$, where the sign of $\mathcal{D}_{12}^x$ can be changed by the polarization δ. Thus, the light-induced interaction favors the spin configuration consisting of the superposition of the collinear configuration along the z axis and the coplanar configuration on the xy plane, which results in the noncoplanar spin configuration with nonzero spin scalar chirality $\chi_{\mathrm{sc}} = \mathbf{S}_1 \cdot \mathbf{S}_2 \times \mathbf{S}_3$. Meanwhile, the sign of χ_{sc} is not determined by $\mathcal{D}_{12}^x$. It is noted that the same light-induced magnetic interactions are also obtained when directly starting from the classical spin model instead of the quantum spin model in Eq. (3) once the Gilbert damping is negligibly small [38,40].

The light-induced symmetric off-diagonal interaction is given by

$$\begin{aligned} \mathcal{H}_{2\mathrm{spin}}^{(2)} &= \mathcal{E}_{12}^y\big[\left(S_1^z S_2^x + S_1^x S_2^z\right) + \left(S_2^{z'} S_3^{x'} + S_2^{x'} S_3^{z'}\right) \\ &\quad + \left(S_3^{z''} S_1^{x''} + S_3^{x''} S_1^{z''}\right)\big] \end{aligned} \tag{50}$$

$$= 3\mathcal{E}_{12}^y\left[m_{A_2'}m_{A_2''} + \frac{1}{\sqrt{2}}\left\{\mathbf{m}_{E_z'} \times \left(2\mathbf{m}_{E_{\mathrm{AFM}}''} - \mathbf{m}_{E_{\mathrm{FM}}''}\right)\right\}^z\right], \tag{51}$$

where $\mathcal{E}_{12}^y = \delta E_0 B_0(-C_{12}^{y;z} + C_{12}^{y;x} - B_{12}^{x;z})/2\Omega$. This interaction belongs to the irreducible representation A_1'' in the point group $m2\overline{6}$ or the totally symmetric irreducible representation in the chiral point group $.23$ as well as the light-induced DM interaction. In the classical spin limit, the symmetric off-diagonal interaction mixes the colinear and coplanar configurations as

$$S^\triangle = \frac{\pm 1}{\sqrt{10}}\big[m_{E_z'}^x S^x(E_z') + m_{E_{\mathrm{AFM}}''}^y S^y(E_{\mathrm{AFM}}'') + m_{E_{\mathrm{FM}}''}^y S^y(E_{\mathrm{FM}}'')\big] \tag{52}$$

where the positive and negative $\mathcal{E}_{12}^y$ favors $S^\triangle$ with $(m_{E_z'}^x, m_{E_{\mathrm{AFM}}''}^y, m_{E_{\mathrm{FM}}''}^y) = (\sqrt{5}, -2, 1)/\sqrt{10}$ and $(m_{E_z'}^x, m_{E_{\mathrm{AFM}}''}^y, m_{E_{\mathrm{FM}}''}^y) = (\sqrt{5}, 2, -1)/\sqrt{10}$, respectively. This spin configuration accompanies nonzero spin scalar chirality, while the sign of χ_{sc} is not determined.

We confirm the above analytical results by using numerical simulation. By starting with a random spin configuration, we calculate a time evolution of the spin scalar chirality χ_{sc} by numerically solving the LLG equation in the classical spin limit ($|\mathbf{S}_i| = 1$). We analyze the Hamiltonian in the LLG equation in Appendix D including only the light-induced DM interaction $\mathcal{H}_{2\mathrm{spin}}^{(1)}$ or symmetric off-diagonal interaction $\mathcal{H}_{2\mathrm{spin}}^{(2)}$ to focus on
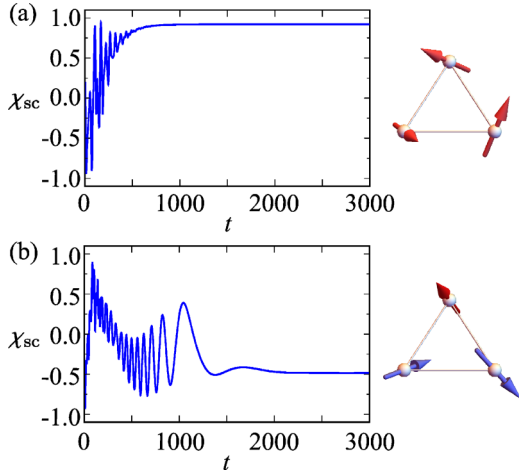
FIG. 6. Time evolutions of the spin scalar chirality χ_{sc} by (a) $\mathcal{D}_{12}^x = 1$ and (b) $\mathcal{E}_{12}^y = 1$. Right panels show the stable spin configurations in each case. The horizontal axis t is the simulation parameter in the LLG equation.

their effect. The time evolution of χ_{sc} and stable spin configurations by $\mathcal{D}_{12}^x = 1$ and $\mathcal{E}_{12}^y = 1$ are shown in Figs. 6(a) and 6(b), respectively. Here, the time t in the horizontal axis is a simulation parameter[3]; the steady state for large t corresponds to the state realized under the light-induced interaction. These numerical results are consistent with the analytical results based on the irreducible representation. Although we obtain the spin configurations with $\chi_{\text{sc}} > 0$ ($\chi_{\text{sc}} < 0$) by $\mathcal{D}_{12}^x$ ($\mathcal{E}_{12}^y$), we also obtain the spin configurations with the opposite χ_{sc} by starting from different random spin configurations. It is noted that the stable spin configuration in Fig. 6(b) has small contributions from bases other than $S^x(E_z')$, $S^y(E_{\text{AFM}}'')$, and $S^y(E_{\text{FM}}'')$ to satisfy the fixed-spin-length condition at each site. The results show the tendency of the nonequilibrium steady state toward noncoplanar spin textures with nonzero spin scalar chirality. To identify the nonequilibrium steady state, it is required to solve the LLG equation incorporating both the static and light-induced interactions, as in Ref. [40]. This previous study showed that the driven system reach the nonequilibrium steady state after $t \sim 10^4 J^{-1}$ (the inverse of the static exchange interaction J^{-1} is the picosecond scale).

3. $\mathcal{H}_Q$

We obtain four types of the light-induced two-site three-spin interaction from Tables IV and V as

$$\mathcal{H}_Q^{(1)} = \mathcal{O}_{12}^{(\text{AS})xyz}\big[\big(Q_1^{xy}S_2^z - S_1^zQ_2^{xy}\big) + \big(Q_2^{x'y'}S_3^{z'} - S_2^{z'}Q_3^{x'y'}\big)$$
$$+ \big(Q_3^{x''y''}S_1^{z''} - S_3^{z''}Q_1^{x''y''}\big)\big], \quad (53)$$

$$\mathcal{H}_Q^{(2)} = \mathcal{O}_{12}^{(\text{S})xxz}\big[\big(Q_1^{xx}S_2^z + S_1^zQ_2^{xx}\big) + \big(Q_2^{x'x'}S_3^{z'} + S_2^{z'}Q_3^{x'x'}\big)$$
$$+ \big(Q_3^{x''x''}S_1^{z''} + S_3^{z''}Q_1^{x''x''}\big)\big], \quad (54)$$

---

[3]The unit of time in the system generally corresponds to J^{-1} (the inverse of the static exchange interaction) for the spin Hamiltonian. Meanwhile, it is noted that determining the unit of time in the present system without the static exchange interaction is difficult.

$$\mathcal{H}_Q^{(3)} = \mathcal{O}_{12}^{(\text{S})yyz}\big[\big(Q_1^{yy}S_2^z + S_1^zQ_2^{yy}\big) + \big(Q_2^{y'y'}S_3^{z'} + S_2^{z'}Q_3^{y'y'}\big)$$
$$+ \big(Q_3^{y''y''}S_1^{z''} + S_3^{z''}Q_1^{y''y''}\big)\big], \quad (55)$$

$$\mathcal{H}_Q^{(4)} = \mathcal{O}_{12}^{(\text{S})wz}\big[\big(Q_1^{zx}S_2^x + S_1^xQ_2^{zx}\big) + \big(Q_2^{z'x'}S_3^{x'} + S_2^{x'}Q_3^{z'x'}\big)$$
$$+ \big(Q_3^{z''x''}S_1^{x''} + S_3^{x''}Q_1^{z''x''}\big)\big]$$
$$- \mathcal{O}_{12}^{(\text{S})wz}\big[\big(Q_1^{yz}S_2^y + S_1^yQ_2^{zy}\big) + \big(Q_2^{y'z'}S_3^{y'} + S_2^{y'}Q_3^{z'y'}\big)$$
$$+ \big(Q_3^{y''z''}S_1^{y''} + S_3^{y''}Q_1^{z''y''}\big)\big]. \quad (56)$$

where $\mathcal{O}_{12}^{(\text{AS})xyz} = \delta E_0^2 B_{12}^{x;z}A_{12}^{y;z}/\Omega$, $\mathcal{O}_{12}^{(\text{S})xxz} = -\delta E_0^2 B_{12}^{x;z}C_{12}^{y;x}/2\Omega$, $\mathcal{O}_{12}^{(\text{S})yyz} = \delta E_0^2 B_{12}^{x;z}C_{12}^{y;y}/2\Omega$, and $\mathcal{O}_{12}^{(\text{S})wz} = \mathcal{O}_{12}^{(\text{S})zxx} = -\mathcal{O}_{12}^{(\text{S})yzy} = \delta E_0^2 B_{12}^{x;z}C_{12}^{y;z}/2\Omega$. As shown in Sec. III B, the light-induced two-site three-spin interaction on the $\langle 1, 2 \rangle$ bond results from the breakings of the twofold rotation C_{y2} and m_x by light. Meanwhile, the triangle system is invariant under the threefold rotation around the z axis. Accordingly, the obtained two-site three-spin interactions belong to the irreducible representation A_2' with the odd parity for $\{C_{y2}, m_x\}$ and the even parity for C_{z3}, as shown in Table VII. It is noted that these interactions on the $\langle 1, 2 \rangle$ bond (the triangle) belongs to the totally symmetric irreducible representation of the black and white magnetic point group $\mathbf{M} = m'2'm$ ($\mathbf{M} = m'2'\bar{6}$). These interactions can be expressed in the ternary of the order parameters, while it is cumbersome to analytically obtain the stable spin configuration.

We directly investigate stable spin configurations by numerically solving the LLG equation in the same manner in Sec. IV B 2. The time evolutions of χ_{sc} and stable spin configurations by setting $\mathcal{O}_{12}^{(\text{AS})xyz} = 1$, $\mathcal{O}_{12}^{(\text{S})xxz} = 1$, $\mathcal{O}_{12}^{(\text{S})yyz} = 1$, or $\mathcal{O}_{12}^{(\text{S})wz} = 1$ are shown in Figs. 7(a)–7(d), respectively. The results show that all the two-site three-spin interactions favor noncoplanar spin configurations with nonzero spin scalar chirality. This is because the spin scalar chirality also belongs to A_2' as well as the two-site three-spin interactions. The mechanism of nonzero χ_{sc} is different from the light-induced two-site two-spin interaction; the two-site two-spin interaction mixes the z spin and the xy spin as a result of the breaking of the horizontal mirror symmetry, while the two-site three-spin interaction is directly coupled to the spin scalar chirality belonging to the same representation. It is noted that the sign of χ_{sc} is not determined by these interactions.

4. $\mathcal{H}_{\text{3site}}$

Next, let us discuss the three-site three-spin interaction under the point group $\mathbf{G} = m2\bar{6}$, where we obtain three types of the interactions as a consequence of the symmetry reduction from the point group $\mathbf{G} = m2\bar{6}$ to the black and white magnetic point group $\mathbf{M} = m'2'\bar{6}$. The obtained three-site three-spin interactions are given by

$$\mathcal{H}_{\text{3site}}^{(1)} = \mathcal{T}^{(1)}\mathbf{S}_1 \cdot \mathbf{S}_2 \times \mathbf{S}_3, \quad (57)$$

$$\mathcal{H}_{\text{3site}}^{(2)} = \mathcal{T}^{(2)}\big[S_1^z\big(S_2^xS_3^x + S_2^yS_3^y\big) + S_2^z\big(S_3^xS_1^x + S_3^yS_1^y\big)$$
$$+ S_3^z\big(S_1^xS_2^x + S_1^yS_2^y\big)\big], \quad (58)$$

$$\mathcal{H}_{\text{3site}}^{(3)} = \mathcal{T}^{(3)}\big[S_1^{z'}\big(S_2^{x'}S_3^{x'} - S_2^{y'}S_3^{y'}\big) + S_2^{z'}\big(S_3^{x''}S_1^{x''} - S_3^{y''}S_1^{y''}\big)$$
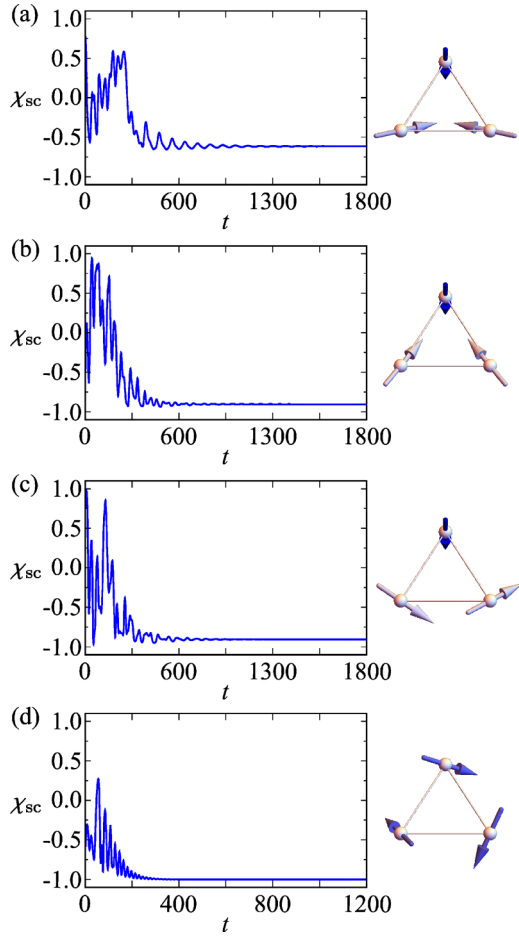$$+ S_3^z\big(S_1^xS_2^x - S_1^yS_2^y\big)\big], \quad (59)$$

FIG. 7. Time evolutions of the spin scalar chirality χ_{sc} by (a) $\mathcal{O}_{12}^{(AS)xyz} = 1$, (b) $\mathcal{O}_{12}^{(S)xxz} = 1$, (c) $\mathcal{O}_{12}^{(S)yyz} = 1$, and (d) $\mathcal{O}_{12}^{(S)wz} = 1$. Right panels show the stable spin configurations in each case. The horizontal axis t is the simulation parameter in the LLG equation.

with

$$\frac{2\Omega}{\delta E_0^2} \mathcal{T}^{(1)} = \frac{\sqrt{3}}{2}(A_{12}^{y;z})^2 - \frac{\sqrt{3}}{4}(B_{12}^{x;z})^2 - \frac{\sqrt{3}}{2}(C_{12}^{y;u})^2$$
$$- \sqrt{3}C_{12}^{y;u}C_{12}^{y;z} + \frac{\sqrt{3}}{2}B_{12}^{x;z}C_{12}^{y;v} - \frac{\sqrt{3}}{4}(C_{12}^{y;v})^2, \quad (60)$$

$$\frac{2\Omega}{\delta E_0^2} \mathcal{T}^{(2)} = -\frac{3}{4}(B_{12}^{x;z})^2 - \sqrt{3}C_{12}^{y;u}A_{12}^{y;z} + \sqrt{3}A_{12}^{y;z}C_{12}^{y;z}$$
$$- \frac{1}{2}B_{12}^{x;z}C_{12}^{y;v} - \frac{3}{4}(C_{12}^{y;v})^2, \quad (61)$$

$$\frac{2\Omega}{\delta E_0^2} \mathcal{T}^{(3)} = \frac{\sqrt{3}}{4}B_{12}^{x;z}A_{12}^{x;z} - \frac{1}{4}B_{12}^{x;z}C_{12}^{y;u} - \frac{1}{2}B_{12}^{x;z}C_{12}^{y;z}$$
$$+ \frac{\sqrt{3}}{4}A_{12}^{x;z}C_{12}^{y;v} + \frac{3}{4}C_{12}^{y;u}C_{12}^{y;v}. \quad (62)$$

Here, $C_{12}^{y;u} = (C_{12}^{y;x} + C_{12}^{y;y})/2$ and $C_{12}^{y;v} = (C_{12}^{y;x} - C_{12}^{y;y})/2$. These interactions are classified into the irreducible representation A_2' under the point group $\mathbf{G} = m2\bar{6}$, i.e., the totally symmetric irreducible representation under the black and white magnetic point group $\mathbf{M} = m'2'\bar{6}$.

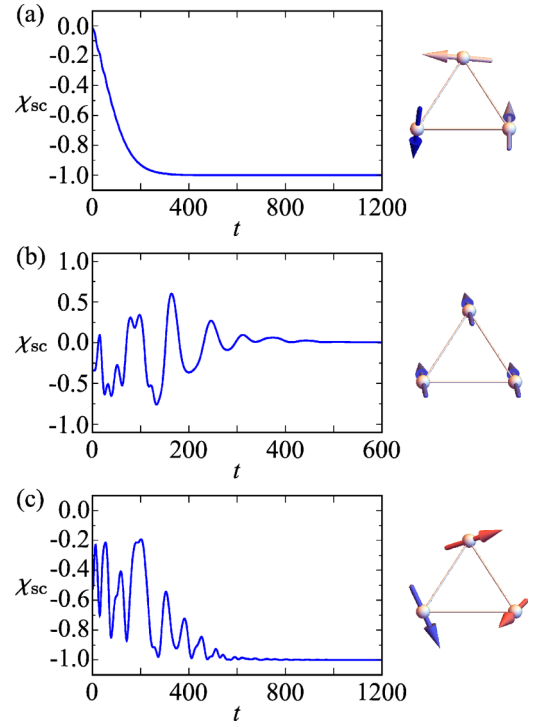FIG. 8. Time evolutions of the spin scalar chirality χ_{sc} by (a) $\mathcal{T}^{(1)} = 1$, (b) $\mathcal{T}^{(2)} = 1$, and (c) $\mathcal{T}^{(3)} = 1$. Right panels show the stable spin configurations in each case. The horizontal axis t is the simulation parameter in the LLG equation.

The stable spin configurations are investigated by numerically solving the LLG equation in the same manner in Sec. IV B 2. Figures 8(a)–8(c) show the time evolutions of χ_{sc} and stable spin configurations by $\mathcal{T}^{(1)} = 1$, $\mathcal{T}^{(2)} = 1$, or $\mathcal{T}^{(3)} = 1$, respectively. We find that $\mathcal{T}^{(1)}$ and $\mathcal{T}^{(3)}$ favor noncoplanar spin configurations with nonzero spin scalar chirality, while $\mathcal{T}^{(2)}$ favors the collinear spin configuration without the spin scalar chirality but with the uniform out-of-plane magnetization. Thus, the three-site three-spin interactions also favor the spin configurations belonging to A_2', which is similar to the situation under the two-site three-spin interactions in Sec. IV B 3. Among $\mathcal{T}$, the mechanism of nonzero χ_{sc} is described by the coupling between these interactions and the spin scalar chirality, as clearly shown in $\mathcal{H}_{3\text{site}}^{(1)}$. The sign of χ_{sc} is fixed by $\mathcal{T}^{(1)}$, while not fixed by $\mathcal{T}^{(3)}$.

V. SUMMARY

To summarize, we have investigated the relation between light-induced magnetic interactions and symmetry lowering by light. By adopting Floquet formalism, we have systematically shown the light-induced two-spin and three-spin interactions for all the crystallographic point groups in two-dimensional insulating magnets. In particular, the light-induced DM interaction ubiquitously appears for all the point groups, which means the possibility to stabilize helical and skyrmion states in any crystal structures. Based on the symmetry argument, we have revealed that the light-induced two-spin and three-spin interactions are the consequence of the reduction from the point group to the chiral point group and the

TABLE VIII. Bond symmetry **G** for the $\langle 1, 2 \rangle$ bond along the x direction on the triangular lattice [TL] [square lattice (SL)] in the hexagonal (tetragonal) point groups. The first, second, and third axes in **G** (hexagonal/tetragonal point groups) are [100], [010], and [001] ([001], [100], and [010]), respectively.

G	site symmetry of TL	site symmetry of SL
mmm	$6/mmm$	$4/mmm$
$2mm$	$\bar{6}2m$	
$m2m$	$\bar{6}m2$	
$mm2$	$6mm$	$4mm, \bar{4}m2$
222	622	$422, \bar{4}2m$
$2/m..$	$\bar{3}m1$	
$.2/m.$	$\bar{3}1m$	
$..2/m$	$6/m..$	$4/m..$
$m..$	$3m1$	
$.m.$	$31m$	
$..m$	$\bar{6}..$	
$2..$	321	
$.2.$	312	
$..2$	$6..$	$4.., \bar{4}..$
$\bar{1}$	$\bar{3}..$	
1	$3..$	

black and white magnetic point group, respectively. These results have uncovered the effect of symmetry lowering by light on magnetic interactions. We have also shown that the light-induced magnetic interactions on the $m2m$ triangular unit favor noncoplanar spin textures with nonzero spin scalar chirality as an example. Our results will give a symmetry-based understanding of controlling magnetic interactions and enable systematic Floquet engineering of magnetic structures based on crystal symmetry.

APPENDIX A: CORRESPONDENCE TO TWO-DIMENSIONAL HEXAGONAL AND TETRAGONAL SYSTEMS

We present the correspondence between the bond symmetry **G** for the $\langle 1, 2 \rangle$ bond and the hexagonal/tetragonal point groups in the lattice systems in Table VIII. For simplicity, we consider the simple triangular (square) lattices with the primitive translation vectors $\boldsymbol{e}_1 = (1, 0, 0)$ and $\boldsymbol{e}_2 = (1/2, \sqrt{3}/2, 0)$ [$\boldsymbol{e}_1 = (1, 0, 0)$ and $\boldsymbol{e}_2 = (0, 1, 0)$], and take the $\langle 1, 2 \rangle$ bond along the x direction. Then, the bond symmetry corresponds to mmm and its subgroups depending on the site (bond) symmetry at each lattice site. There are sixteen patterns of **G** for the hexagonal point groups (including the trigonal point groups) and five patterns for the tetragonal point groups, as shown in Table VIII.

APPENDIX B: COUPLING MATRIX AND THIRD-RANK ME TENSOR IN THE GLOBAL CARTESIAN SPIN COORDINATE

We show the coupling matrix and third-rank ME tensor in Sec. IV in the global Cartesian spin coordinate, which are given by

$$
J_{12} = \begin{pmatrix} F^x & D^z & 0 \\ -D^z & F^y & 0 \\ 0 & 0 & F^z \end{pmatrix}, \quad
J_{23} = \begin{pmatrix} \frac{1}{4}(F^x + 3F^y) & \frac{\sqrt{3}}{4}(-F^x + F^y) + D^z & 0 \\ \frac{\sqrt{3}}{4}(-F^x + F^y) - D^z & \frac{1}{4}(3F^x + F^y) & 0 \\ 0 & 0 & F^z \end{pmatrix}, \tag{B1}
$$

$$
J_{31} = \begin{pmatrix} \frac{1}{4}(F^x + 3F^y) & \frac{\sqrt{3}}{4}(F^x - F^y) + D^z & 0 \\ \frac{\sqrt{3}}{4}(F^x - F^y) - D^z & \frac{1}{4}(3F^x + F^y) & 0 \\ 0 & 0 & F^z \end{pmatrix}, \quad
Y_{12}^x = \begin{pmatrix} 0 & B_{12}^{x;z} & 0 \\ B_{12}^{x;z} & 0 & 0 \\ 0 & 0 & 0 \end{pmatrix}, \quad
Y_{12}^y = \begin{pmatrix} C_{12}^{y;x} & A_{12}^{y;z} & 0 \\ -A_{12}^{y;z} & C_{12}^{y;y} & 0 \\ 0 & 0 & C_{12}^{y;z} \end{pmatrix}, \tag{B2}
$$

$$
Y_{23}^x = \begin{pmatrix} -\frac{\sqrt{3}}{8}\left(C_{12}^{y;x} + 3C_{12}^{y;y} + 2B_{12}^{x;z}\right) & \frac{1}{8}\left(3C_{12}^{y;x} - 3C_{12}^{y;y} + 2B_{12}^{x;z}\right) - \frac{\sqrt{3}}{2}A_{12}^{y;z} & 0 \\ \frac{1}{8}\left(3C_{12}^{y;x} - 3C_{12}^{y;y} + 2B_{12}^{x;z}\right) + \frac{\sqrt{3}}{2}A_{12}^{y;z} & -\frac{\sqrt{3}}{8}\left(3C_{12}^{y;x} + C_{12}^{y;y} - 2B_{12}^{x;z}\right) & 0 \\ 0 & 0 & -\frac{\sqrt{3}}{2}C_{12}^{y;z} \end{pmatrix}, \tag{B3}
$$

$$
Y_{23}^y = \begin{pmatrix} -\frac{1}{8}\left(C_{12}^{y;x} + 3C_{12}^{y;y} - 6B_{12}^{x;z}\right) & \frac{\sqrt{3}}{8}\left(C_{12}^{y;x} - C_{12}^{y;y} - 2B_{12}^{x;z}\right) - \frac{1}{2}A_{12}^{y;z} & 0 \\ \frac{\sqrt{3}}{8}\left(C_{12}^{y;x} - C_{12}^{y;y} - 2B_{12}^{x;z}\right) + \frac{1}{2}A_{12}^{y;z} & -\frac{1}{8}\left(3C_{12}^{y;x} + C_{12}^{y;y} + 6B_{12}^{x;z}\right) & 0 \\ 0 & 0 & -\frac{1}{2}C_{12}^{y;z} \end{pmatrix}, \tag{B4}
$$

$$
Y_{31}^x = \begin{pmatrix} \frac{\sqrt{3}}{8}\left(C_{12}^{y;x} + 3C_{12}^{y;y} + 2B_{12}^{x;z}\right) & \frac{1}{8}\left(3C_{12}^{y;x} - 3C_{12}^{y;y} + 2B_{12}^{x;z}\right) + \frac{\sqrt{3}}{2}A_{12}^{y;z} & 0 \\ \frac{1}{8}\left(3C_{12}^{y;x} - 3C_{12}^{y;y} + 2B_{12}^{x;z}\right) - \frac{\sqrt{3}}{2}A_{12}^{y;z} & \frac{\sqrt{3}}{8}\left(3C_{12}^{y;x} + C_{12}^{y;y} - 2B_{12}^{x;z}\right) & 0 \\ 0 & 0 & \frac{\sqrt{3}}{2}C_{12}^{y;z} \end{pmatrix}, \tag{B5}
$$

$$Y_{31}^y = \begin{pmatrix} -\frac{1}{8}\left(C_{12}^{y;x} + 3C_{12}^{y;y} - 6B_{12}^{x;z}\right) & -\frac{\sqrt{3}}{8}\left(C_{12}^{y;x} - C_{12}^{y;y} - 2B_{12}^{x;z}\right) - \frac{1}{2}A_{12}^{y;z} & 0 \\ -\frac{\sqrt{3}}{8}\left(C_{12}^{y;x} - C_{12}^{y;y} - 2B_{12}^{x;z}\right) + \frac{1}{2}A_{12}^{y;z} & -\frac{1}{8}\left(3C_{12}^{y;x} + C_{12}^{y;y} + 6B_{12}^{x;z}\right) & 0 \\ 0 & 0 & -\frac{1}{2}C_{12}^{y;z} \end{pmatrix}. \tag{B6}$$

APPENDIX C: BASES OF IRREDUCIBLE REPRESENTATION

The eigenbases $S^\alpha(\Gamma)$ in Fig. 5 are given by

$$S(A_2') = (0, 0, 1, 0, 0, 1, 0, 0, 1), \tag{C1}$$

$$S(A_1'') = \frac{1}{2}(-\sqrt{3}, -1, 0, \sqrt{3}, -1, 0, 0, 2, 0), \tag{C2}$$

$$S(A_2'') = \frac{1}{2}(1, -\sqrt{3}, 0, 1, \sqrt{3}, 0, -2, 0, 0), \tag{C3}$$

$$S^x(E_z') = \frac{1}{\sqrt{2}}(0, 0, -1, 0, 0, -1, 0, 0, 2), \tag{C4}$$

$$S^y(E_z') = \sqrt{\frac{3}{2}}(0, 0, 1, 0, 0, -1, 0, 0, 0), \tag{C5}$$

$$S^x(E_{FM}'') = (0, -1, 0, 0, -1, 0, 0, -1, 0), \tag{C6}$$

$$S^y(E_{FM}'') = (1, 0, 0, 1, 0, 0, 1, 0, 0), \tag{C7}$$

$$S^x(E_{AFM}'') = \frac{1}{2}(\sqrt{3}, -1, 0, -\sqrt{3}, -1, 0, 0, 2, 0), \tag{C8}$$

$$S^y(E_{AFM}'') = \frac{1}{2}(-1, -\sqrt{3}, 0, -1, \sqrt{3}, 0, 2, 0, 0), \tag{C9}$$

where $S^\alpha(\Gamma) \cdot S^\beta(\Gamma') = 3\delta_{\Gamma\Gamma'}\delta_{\alpha\beta}$.

APPENDIX D: LANDAU-LIFSHITZ-GILBERT EQUATION

In classical spin Hamiltonians $\mathcal{H}$, the time evolution of the classical spin ($|S_i| = 1$) at zero temperature is calculated by the LLG equation, which is given by

$$\frac{dS_i}{dt} = -\frac{\gamma}{1+\alpha^2}\left[S_i \times H_i^{\text{eff}} + \alpha S_i \times \left(S_i \times H_i^{\text{eff}}\right)\right] \tag{D1}$$

with the gyromagnetic ratio γ, the Gilbert damping constant α, and the effective magnetic field $H_i^{\text{eff}} = -\partial\mathcal{H}/\partial S_i$. The first term represents the precession of the spin around the effective magnetic field, while the second term takes into account the relaxation of the spin to the effective magnetic field. In the calculation for the effective time-independent Hamiltonians in Sec. IV, the system evolves in time to a lower-energy spin state and finally reaches a stable state owing to the second term. Thus, Figs. 6–8 show the tendency of the nonequilibrium steady state. We search for the nonequilibrium steady state by numerically solving the LLG equation by typically setting $\gamma = 1$ and $\alpha = 0.01$–0.2 and by using an open software DifferentialEquations.jl [47]. It is noted that the finally obtained state is independent of an initial spin configuration, although we start simulations from a random spin configuration.

[1] A. Eckardt, Rev. Mod. Phys. **89**, 011004 (2017).

[2] T. Oka and S. Kitamura, Annu. Rev. Condens. Matter Phys. **10**, 387 (2019).

[3] M. S. Rudner and N. H. Lindner, arXiv:2003.08252.

[4] J. H. Mentink, K. Balzer, and M. Eckstein, Nat. Commun. **6**, 6708 (2015).

[5] J. H. Mentink, J. Phys.: Condens. Matter **29**, 453001 (2017).

[6] J. Liu, K. Hejazi, and L. Balents, Phys. Rev. Lett. **121**, 107201 (2018).

[7] K. Hejazi, J. Liu, and L. Balents, Phys. Rev. B **99**, 205111 (2019).

[8] M. Bukov, M. Kolodrubetz, and A. Polkovnikov, Phys. Rev. Lett. **116**, 125301 (2016).

[9] S. Chaudhary, D. Hsieh, and G. Refael, Phys. Rev. B **100**, 220403(R) (2019).

[10] V. L. Quito and R. Flint, Phys. Rev. Lett. **126**, 177201 (2021).

[11] S. Kitamura, T. Oka, and H. Aoki, Phys. Rev. B **96**, 014406 (2017).

[12] M. Claassen, H.-C. Jiang, B. Moritz, and T. P. Devereaux, Nat. Commun. **8**, 1192 (2017).

[13] V. L. Quito and R. Flint, Phys. Rev. B **103**, 134435 (2021).

[14] S. Sur, A. Udupa, and D. Sen, Phys. Rev. B **105**, 054423 (2022).

[15] J. M. Losada, A. Brataas, and A. Qaiumzadeh, Phys. Rev. B **100**, 060410(R) (2019).

[16] N. Arakawa and K. Yonemitsu, Phys. Rev. B **103**, L100408 (2021).

[17] N. Arakawa and K. Yonemitsu, Phys. Rev. B **104**, 214413 (2021).

[18] P. Strobel and M. Daghofer, Phys. Rev. B **105**, 085144 (2022).

[19] U. Kumar, S. Banerjee, and S.-Z. Lin, Commun. Phys. **5**, 157 (2022).

[20] A. Sriram and M. Claassen, Phys. Rev. Res. **4**, L032036 (2022).

[21] I. Dzyaloshinsky, J. Phys. Chem. Solids **4**, 241 (1958).

[22] T. Moriya, Phys. Rev. **120**, 91 (1960).

[23] M. Sato, Y. Sasaki, and T. Oka, arXiv:1404.2010.

[24] M. Sato, S. Takayoshi, and T. Oka, Phys. Rev. Lett. **117**, 147202 (2016).

[25] S.-W. Cheong and M. Mostovoy, Nat. Mater. **6**, 13 (2007).

[26] Y. Tokura, S. Seki, and N. Nagaosa, Rep. Prog. Phys. **77**, 076501 (2014).

[27] H. Katsura, N. Nagaosa, and A. V. Balatsky, Phys. Rev. Lett. **95**, 057205 (2005).

[28] M. Mostovoy, Phys. Rev. Lett. **96**, 067601 (2006).

[29] I. A. Sergienko and E. Dagotto, Phys. Rev. B **73**, 094434 (2006).

[30] A. B. Harris, T. Yildirim, A. Aharony, and O. Entin-Wohlman, Phys. Rev. B **73**, 184433 (2006).

[31] A. B. Harris, Phys. Rev. B **76**, 054447 (2007).

[32] N. Hur, S. Park, P. A. Sharma, J. S. Ahn, S. Guha, and S.-W. Cheong, Nature (London) **429**, 392 (2004).

[33] Y. J. Choi, H. T. Yi, S. Lee, Q. Huang, V. Kiryukhin, and S.-W. Cheong, Phys. Rev. Lett. **100**, 047601 (2008).

[34] T. A. Kaplan and S. D. Mahanti, Phys. Rev. B **83**, 174432 (2011).

[35] M. Matsumoto, K. Chimata, and M. Koga, J. Phys. Soc. Jpn. **86**, 034704 (2017).

[36] A. Eckardt and E. Anisimovas, New J. Phys. **17**, 093039 (2015).

[37] T. Mikami, S. Kitamura, K. Yasuda, N. Tsuji, T. Oka, and H. Aoki, Phys. Rev. B **93**, 144307 (2016).

[38] T. Hirosawa, J. Klinovaja, D. Loss, and S. A. Díaz, Phys. Rev. Lett. **128**, 037201 (2022).

[39] Y. Tokura and S. Seki, Adv. Mater. **22**, 1554 (2010).

[40] S. Higashikawa, H. Fujita, and M. Sato, arXiv:1810.01103.

[41] R. Mankowsky, M. Först, and A. Cavalleri, Rep. Prog. Phys. **79**, 064503 (2016).

[42] A. S. Disa, T. F. Nova, and A. Cavalleri, Nat. Phys. **17**, 1087 (2021).

[43] S. O. Hanslin and A. Qaiumzadeh, Phys. Rev. B **103**, 134428 (2021).

[44] J.-I. Kishine, H. Kusunose, and H. M. Yamamoto, Isr. J. Chem. **62**, e202200049 (2022).

[45] C. Bradley and A. Cracknell, *The Mathematical Theory of Symmetry in Solids: Representation Theory for Point Groups and Space Groups* (Oxford University Press, Oxford, 2009).

[46] K. Essafi, O. Benton, and L. D. C. Jaubert, Phys. Rev. B **96**, 205126 (2017).

[47] C. Rackauckas and Q. Nie, J. Open Res. Softw. **5**, 15 (2017).